
SOLVING KERNEL RIDGE REGRESSION WITH GRADIENT DESCENT FOR A NON-CONSTANT KERNEL

Oskar Allerbo

Department of Mathematics
KTH Royal Institute of Technology
oallerbo@kth.se

ABSTRACT

Kernel ridge regression, KRR, is a generalization of linear ridge regression that is non-linear in the data, but linear in the parameters. The solution can be obtained either as a closed-form solution, which includes solving a system of linear equations, or iteratively through gradient descent. Using the iterative approach opens up for changing the kernel during training, something that is investigated in this paper. We theoretically address the effects this has on model complexity and generalization. Based on our findings, we propose an update scheme for the bandwidth of translational-invariant kernels, where we let the bandwidth decrease to zero during training, thus circumventing the need for hyper-parameter selection. We demonstrate on real and synthetic data how decreasing the bandwidth during training outperforms using a constant bandwidth, selected by cross-validation and marginal likelihood maximization. We also show theoretically and empirically that using a decreasing bandwidth, we are able to achieve both zero training error in combination with good generalization, and a double descent behavior, phenomena that do not occur for KRR with constant bandwidth but are known to appear for neural networks.

Keywords: Kernel Ridge Regression, Gradient Descent, Hyper-Parameter Selection, Double Descent, Gradient Flow

1 Introduction

Kernel ridge regression, KRR, is a generalization of linear ridge regression that is non-linear in the data, but linear in the parameters. Just as for linear ridge regression, KRR has a closed-form solution, however at the cost of solving a system of n linear equations, where n is the number of training observations. The KRR estimate coincides with the posterior mean of kriging, or Gaussian process regression, (Krige, 1951; Matheron, 1963) and has successfully been applied within a wide range of applications (Zahrt et al., 2019; Ali et al., 2020; Chen and Leclair, 2021; Fan et al., 2021; Le et al., 2021; Safari and Rahimzadeh Arashloo, 2021; Shahsavari et al., 2021; Singh Alvarado et al., 2021; Wu et al., 2021; Chen et al., 2022).

Solving kernel regression with gradient descent, something we refer to as kernel gradient descent, KGD, but which is also known as functional gradient descent (Mason et al., 1999), has been studied by e.g. Yao et al. (2007), Raskutti et al. (2014), Ma and Belkin (2017), and Allerbo (2023). The algorithm requires $\mathcal{O}(Tn^2)$ operations, where T is the number of iterations and n is the number of observations, which, for problems where T is smaller than n , is computationally more efficient than the $\mathcal{O}(n^3)$ operations required for solving the system of linear equations of the closed-form solution.

In addition to computational efficiency, the theoretical understandings from solving simpler regression problems, such as kernel regression, using gradient-based methods can be used for a deeper understanding of more complex regression models, such as neural networks (Belkin et al., 2018; Bartlett et al., 2021). Perhaps counter-intuitively, overparameterized neural networks, where the number of parameters is larger than the number of observations, tend to generalize well (Zhang et al., 2021), a phenomenon often referred to as double descent (Belkin et al., 2019; Advani et al., 2020). Jacot et al. (2018) showed that for highly overparameterized neural networks, the model updates are virtually linear in the parameters, with perfect linearity when the number of parameters goes to infinity. That is, the network is linear in the parameters, but non-linear in the data, just as for kernel regression. In fact, a neural network

that is linear in its parameters can equivalently be expressed as a kernel regression problem, with a kernel that is a function of the network architecture and the parameter values at initialization. The authors refer to this kernel as the neural tangent kernel. Training a (highly) overparameterized neural network with gradient descent is thus (basically) equivalent to solving kernel regression with gradient descent.

Both the neural tangent kernel interpretation and the solutions of KGD, assume that the kernel is constant during training. However, for neural networks with finitely many parameters, this is not the case. Furthermore, the model complexity of neural networks is known to increase with training (Kalimeris et al., 2019). Thus, training a neural network can be thought of as KGD with a kernel whose complexity increases during training.

In this paper, we introduce kernel gradient descent with a non-constant kernel, whose complexity increases during training. In Section 2, we review KRR, KGD, and kernel gradient flow, KGF, which is how we refer to KGD with infinitesimal optimization step size. In Section 3, we analyze KGD and KGF for non-constant kernels in terms of generalization and model complexity. Based on these analyses, we propose an update scheme for the bandwidth of translational-invariant kernels. In Section 4, we theoretically analyze the double descent phenomenon for KGD with non-constant bandwidth. In Section 5, we empirically verify our theoretical results on real and synthetic data.

Our main contributions are listed below.

- We analyze the generalization properties of KGD with a non-constant kernel.
- For translational-invariant kernels we
 - present a theoretically justified kernel update scheme for the bandwidth.
 - theoretically analyze the occurrence of double descent.
- We demonstrate on five real data sets that, compared to a constant bandwidth, a non-constant bandwidth leads to
 - better model performance.
 - zero training error in combination with good generalization.
 - a double descent behavior.

All proofs are deferred to Appendix B.

2 Review of Kernel Ridge Regression, Kernel Gradient Descent and Kernel Gradient Flow

For a positive semi-definite kernel function, $k(\mathbf{x}, \mathbf{x}') \in \mathbb{R}$, and n paired observations, $(\mathbf{x}_i, y_i)_{i=1}^n \in \mathbb{R}^p \times \mathbb{R}$, presented in a design matrix, $\mathbf{X} = [\mathbf{x}_1^\top, \mathbf{x}_2^\top, \dots, \mathbf{x}_n^\top]^\top \in \mathbb{R}^{n \times p}$, and a response vector, $\mathbf{y} \in \mathbb{R}^n$, and for a given regularization strength, $\lambda > 0$, the objective function, and the predictions, of kernel ridge regression, KRR, are given by

$$\hat{\boldsymbol{\alpha}} = \arg \min_{\boldsymbol{\alpha} \in \mathbb{R}^n} \frac{1}{2} \|\mathbf{y} - \mathbf{K} \boldsymbol{\alpha}\|_2^2 + \frac{\lambda}{2} \|\boldsymbol{\alpha}\|_{\mathbf{K}}^2 = (\mathbf{K} + \lambda \mathbf{I})^{-1} \mathbf{y},$$

$$\begin{bmatrix} \hat{\mathbf{f}} \\ \hat{\mathbf{f}}^* \end{bmatrix} = \begin{bmatrix} \mathbf{K} \\ \mathbf{K}^* \end{bmatrix} \hat{\boldsymbol{\alpha}} = \begin{bmatrix} \mathbf{K} \\ \mathbf{K}^* \end{bmatrix} (\mathbf{K} + \lambda \mathbf{I})^{-1} \mathbf{y}. \quad (1)$$

Here, the two kernel matrices $\mathbf{K} = \mathbf{K}(\mathbf{X}) \in \mathbb{R}^{n \times n}$ and $\mathbf{K}^* = \mathbf{K}^*(\mathbf{X}^*, \mathbf{X}) \in \mathbb{R}^{n^* \times n}$ are defined according to $\mathbf{K}_{ij} = k(\mathbf{x}_i, \mathbf{x}_j)$ and $\mathbf{K}_{ij}^* = k(\mathbf{x}_i^*, \mathbf{x}_j)$, where $\mathbf{X}^* = [\mathbf{x}_1^{*\top}, \mathbf{x}_2^{*\top}, \dots, \mathbf{x}_{n^*}^{*\top}]^\top \in \mathbb{R}^{n^* \times p}$ denotes new data. The vectors $\hat{\mathbf{f}} = \hat{\mathbf{f}}(\mathbf{X}) = [\hat{f}(\mathbf{x}_1), \hat{f}(\mathbf{x}_2), \dots, \hat{f}(\mathbf{x}_n)]^\top \in \mathbb{R}^n$ and $\hat{\mathbf{f}}^* = \hat{\mathbf{f}}^*(\mathbf{X}^*, \mathbf{X}) = [\hat{f}(\mathbf{x}_1^*), \hat{f}(\mathbf{x}_2^*), \dots, \hat{f}(\mathbf{x}_{n^*}^*)]^\top \in \mathbb{R}^{n^*}$ denote model predictions on training and new data, respectively. For a single prediction, $\hat{f}(\mathbf{x}^*) \in \hat{\mathbf{f}}^*$, $\hat{f}(\mathbf{x}^*) = \hat{f}(\mathbf{x}^*, \lambda) = \mathbf{k}^{*\top} (\mathbf{K} + \lambda \mathbf{I})^{-1} \mathbf{y}$, where $\mathbf{k}^* = \mathbf{k}^*(\mathbf{x}^*, \mathbf{X}) \in \mathbb{R}^n$, and $\mathbf{k}^*(\mathbf{x}^*, \mathbf{X})^\top$ is the row in \mathbf{K}^* corresponding to \mathbf{x}^* . The weighted norm, $\|\mathbf{v}\|_{\mathbf{A}}$, is defined according to $\|\mathbf{v}\|_{\mathbf{A}}^2 = \mathbf{v}^\top \mathbf{A} \mathbf{v}$ for any symmetric positive definite matrix \mathbf{A} .

The similarities between ridge regression and gradient descent with early stopping are well studied for linear regression (Friedman and Popescu, 2004; Ali et al., 2019; Allerbo et al., 2023). In the context of early stopping, optimization time can be thought of as an inverse penalty, where longer optimization time corresponds to weaker regularization. For gradient descent with infinitesimal step size, often referred to as gradient flow, a closed-form solution exists that allows for direct comparisons to ridge regression. The generalization of gradient flow from the linear to the kernel setting was studied by Allerbo (2023), who used the names kernel gradient descent, KGD, and kernel gradient flow, KGF. Sometimes, the name functional gradient descent is used rather than KGD.

The update rule for KGD, with step size η , is given by

$$\begin{bmatrix} \hat{\mathbf{f}} \\ \hat{\mathbf{f}}^* \end{bmatrix}_{k+1} = \begin{bmatrix} \hat{\mathbf{f}} \\ \hat{\mathbf{f}}^* \end{bmatrix}_k + \eta \cdot \begin{bmatrix} \mathbf{K} \\ \mathbf{K}^* \end{bmatrix} (\mathbf{y} - \hat{\mathbf{f}}_k), \quad \begin{bmatrix} \hat{\mathbf{f}} \\ \hat{\mathbf{f}}^* \end{bmatrix}_0 = \begin{bmatrix} \boldsymbol{\mu} \\ \boldsymbol{\mu}^* \end{bmatrix}, \quad (2)$$

where $[\boldsymbol{\mu}^\top, \boldsymbol{\mu}^{*\top}]^\top = [\boldsymbol{\mu}(\mathbf{X})^\top, \boldsymbol{\mu}^*(\mathbf{X}^*)^\top]^\top$ for some prior function $\mu(\mathbf{x})$.

The KGF solution is obtained by treating Equation 2 as the Euler forward formulation of the differential equation in Equation 3,

$$\frac{\partial}{\partial t} \begin{bmatrix} \hat{\mathbf{f}}(t) \\ \hat{\mathbf{f}}^*(t) \end{bmatrix} = \begin{bmatrix} \mathbf{K} \\ \mathbf{K}^* \end{bmatrix} (\mathbf{y} - \hat{\mathbf{f}}(t)), \quad \begin{bmatrix} \hat{\mathbf{f}}(0) \\ \hat{\mathbf{f}}^*(0) \end{bmatrix} = \begin{bmatrix} \boldsymbol{\mu} \\ \boldsymbol{\mu}^* \end{bmatrix}, \quad (3)$$

whose solution is given by

$$\begin{bmatrix} \hat{\mathbf{f}}(t) \\ \hat{\mathbf{f}}^*(t) \end{bmatrix} = \begin{bmatrix} \mathbf{I} \\ \mathbf{K}^* \mathbf{K}^{-1} \end{bmatrix} (\mathbf{I} - \exp(-t\mathbf{K})) (\mathbf{y} - \boldsymbol{\mu}) + \begin{bmatrix} \boldsymbol{\mu} \\ \boldsymbol{\mu}^* \end{bmatrix}, \quad (4)$$

where \exp denotes the matrix exponential.

Remark 1: Note that $\mathbf{K}^{-1}(\mathbf{I} - \exp(-t\mathbf{K})) = (\mathbf{I} - \exp(-t\mathbf{K}))\mathbf{K}^{-1}$ is well-defined even when \mathbf{K} is singular. The matrix exponential is defined through its Taylor approximation and from $\mathbf{I} - \exp(-t\mathbf{K}) = t\mathbf{K} - \frac{1}{2}t^2\mathbf{K}^2 + \dots$, a matrix \mathbf{K} factors out, that cancels with \mathbf{K}^{-1} .

Remark 2: For KGD, the prior function, $\mu(\mathbf{x})$, is trivially incorporated as the initialization vector $[\boldsymbol{\mu}^\top, \boldsymbol{\mu}^{*\top}]^\top$. For KRR, the prior function can be included by shifting both \mathbf{y} and f with it, i.e. by replacing \mathbf{y} and $[\hat{\mathbf{f}}^\top, \hat{\mathbf{f}}^{*\top}]^\top$ by $\mathbf{y}_\mu := \mathbf{y} - \boldsymbol{\mu}$ and $[\hat{\mathbf{f}}_\mu^\top, \hat{\mathbf{f}}_{\mu}^{*\top}]^\top := [(\hat{\mathbf{f}} - \boldsymbol{\mu})^\top, (\hat{\mathbf{f}}^* - \boldsymbol{\mu}^*)^\top]^\top$ in Equation 1. To alleviate notation, we henceforth use the prior shifted observations and predictions also for KGD/KGF, rewriting Equations 2 and 4 as

$$\begin{bmatrix} \hat{\mathbf{f}}_\mu \\ \hat{\mathbf{f}}_{\mu}^* \end{bmatrix}_{k+1} = \begin{bmatrix} \hat{\mathbf{f}}_\mu \\ \hat{\mathbf{f}}_{\mu}^* \end{bmatrix}_k + \eta \cdot \begin{bmatrix} \mathbf{K} \\ \mathbf{K}^* \end{bmatrix} (\mathbf{y} - \hat{\mathbf{f}}_{\mu,k}), \quad \begin{bmatrix} \hat{\mathbf{f}}_\mu \\ \hat{\mathbf{f}}_{\mu}^* \end{bmatrix}_0 = \mathbf{0} \quad (5)$$

and

$$\begin{bmatrix} \hat{\mathbf{f}}_\mu(t) \\ \hat{\mathbf{f}}_{\mu}^*(t) \end{bmatrix} = \begin{bmatrix} \mathbf{I} \\ \mathbf{K}^* \mathbf{K}^{-1} \end{bmatrix} (\mathbf{I} - \exp(-t\mathbf{K})) \mathbf{y}_\mu. \quad (6)$$

3 Kernel Gradient Descent with Non-Constant Kernels

If we allow for $[\mathbf{K}^\top \mathbf{K}^{*\top}]^\top$ to vary between time steps in Equation 5, we obtain KGD with a non-constant kernel. Below, we theoretically analyze the effects of this, discuss the implications for generalization, and propose an algorithm for kernel update during training.

We base our analysis of generalization on the axiom that for generalization to be good, the inferred function should deviate roughly as much from the prior function as the training data does. That is, if the training data follows the prior closely, so should the inferred function, and if the training data deviates from the prior, so should the inferred function.

Axiom 1.

For generalization to be good, the deviation between the inferred function and the prior should be of the same order as the deviation between the training data and the prior.

Axiom 1 is violated if, for $y_{\mu,i} = (\mathbf{y}_\mu)_i$ and $\hat{f}_\mu(\mathbf{x}^*) \in \hat{\mathbf{f}}_{\mu}^*$,

- $|\hat{f}_\mu(\mathbf{x}^*)| \ll \min_i |y_{\mu,i}|$ for a large part of the predictions (predictions follow the prior too closely), or if
- $|\hat{f}_\mu(\mathbf{x}^*)| \gg \max_i |y_{\mu,i}|$ for a large part of the predictions (predictions are too extreme).

Remark 1: The implications of Axiom 1 are probably most intuitive for a zero prior. Then “predictions follow the prior too closely” simply means “the model predicts mostly zero”.

Remark 2: In the following, we will treat Axiom 1 qualitatively rather than quantitatively, i.e. we will not exactly quantize the concepts “large”, “small”, “close”, and so on.

3.1 Generalization for Non-Constant Kernels

In order to evaluate Axiom, we would like to relate $|\hat{f}_\mu(\mathbf{x}^*)|$ and $\|\mathbf{y}_\mu\|$. For a constant kernel, this can be obtained from the closed form solutions of Equations 1 and 6; in Lemma 1, we bound the quotients of the two quantities.

Lemma 1.

$$\hat{f}_\mu(\mathbf{x}^*, t) = \mathbf{k}^{*\top} (\mathbf{I} - \exp(-t\mathbf{K}))\mathbf{K}^{-1}\mathbf{y}_\mu \implies |\hat{f}_\mu(\mathbf{x}^*, t)| \leq \|\mathbf{k}^*\|_2 \cdot \min\left(t, \frac{1}{s_{\min}}\right) \cdot \|\mathbf{y}_\mu\|_2, \quad (7a)$$

$$\hat{f}_\mu(\mathbf{x}^*, \lambda) = \mathbf{k}^{*\top} (\mathbf{K} + \lambda\mathbf{I})^{-1}\mathbf{y}_\mu \implies |\hat{f}_\mu(\mathbf{x}^*, \lambda)| \leq \|\mathbf{k}^*\|_2 \cdot \min\left(\frac{1}{\lambda}, \frac{1}{s_{\min}}\right) \cdot \|\mathbf{y}_\mu\|_2, \quad (7b)$$

where $s_{\min} = s_{\min}(\mathbf{K})$ denotes the smallest singular value of \mathbf{K} .

Remark 1: Since \mathbf{K} is a symmetric, positive semi-definite matrix, its eigenvalues and singular values coincide. To avoid confusion with the regularization parameter, λ , and to emphasize that $\lambda_{\min}(\mathbf{K}) = s_{\min}(\mathbf{K}) \geq 0$, we will use the term singular values henceforth.

Remark 2: Equation 7 suggests that t and λ are connected as $t = 1/\lambda$. This is also the relation proposed in previous work on the similarities between (kernel) ridge regression and (kernel) gradient flow.

However, when we allow the kernel to change during training, there in general is no closed-form solution to Equation 3, and we cannot use the bound in Equation 7a. However, in Proposition 1 we present a generalization of the KGF bound that also holds for non-constant kernels, despite the absence of a closed-form solution for $\hat{f}(\mathbf{x}^*, t)$.

Proposition 1.

Let $\overline{k}_2^*(t)$ denote the weighted average of $\|\mathbf{k}^*(\tau)\|_2$ during training, with weight function $\|\mathbf{y} - \hat{\mathbf{f}}(\tau)\|_2$, and let $s_{\min}(t)$ denote the smallest singular value of $\mathbf{K}(t)$, i.e.

$$\overline{k}_2^*(t) := \frac{\int_0^t \|\mathbf{k}^*(\tau)\|_2 \cdot \|\mathbf{y} - \hat{\mathbf{f}}(\tau)\|_2 d\tau}{\int_0^t \|\mathbf{y} - \hat{\mathbf{f}}(\tau)\|_2 d\tau} \quad \text{and} \quad s_{\min}(t) := s_{\min}(\mathbf{K}(t)).$$

Then, for the KGF estimate, $\hat{f}_\mu(\mathbf{x}^*, t)$, for some $t' \in [0, t]$,

$$|\hat{f}_\mu(\mathbf{x}^*, t)| \leq \overline{k}_2^*(t) \cdot \min\left(t, \frac{1}{s_{\min}(t')}\right) \cdot \|\mathbf{y}_\mu\|_2. \quad (8)$$

Remark 1: Note that $\mathbf{y} - \hat{\mathbf{f}} = \mathbf{y} - \boldsymbol{\mu} - (\hat{\mathbf{f}} - \boldsymbol{\mu}) = \mathbf{y}_\mu - \hat{\mathbf{f}}_\mu$.

Remark 2: For a constant kernel, $s_{\min}(t') = s_{\min}$ and $\overline{k}_2^*(t) = \|\mathbf{k}^*\|_2$ and Equation 8 reduces to Equation 7a.

The first criterion of Axiom 1 is violated if $|\hat{f}_\mu(\mathbf{x}^*, t)| \ll \|\mathbf{y}_\mu\|_2$, which can be obtained either through a small value of $\overline{k}_2^*(t)$, a large value of $s_{\min}(t')$, or a small value of t . The second criterion is violated if $|\hat{f}_\mu(\mathbf{x}^*, t)| \gg \|\mathbf{y}_\mu\|_2$, which can be obtained either through a large value of $\overline{k}_2^*(t)$, or a small value of $s_{\min}(t')$ in combination with a large value of t . Let us consider a translational-invariant, decreasing kernel of the form $k(\mathbf{x}, \mathbf{x}', \sigma(\tau)) = k\left(\frac{1}{\sigma(\tau)} \cdot \|\mathbf{x} - \mathbf{x}'\|_{\Theta}\right) = k\left((\mathbf{x} - \mathbf{x}')^\top \cdot \frac{1}{\sigma(\tau)} \Theta \cdot (\mathbf{x} - \mathbf{x}')\right)$, such that $k(0) = 1$, $k(\infty) = 0$, and $k'(u) \leq 0$, where $\Theta = \Sigma^{-1} \in \mathbb{R}^{p \times p}$ (and $\frac{1}{\sigma(\tau)} \Theta = (\sigma(\tau)\Sigma)^{-1}$) for some positive definite covariance matrix $\sigma(\tau)\Sigma$. Then $\overline{k}_2^*(t) \in [0, \sqrt{n}]$ is small if σ is small during the early stages of training, but it can never be larger than \sqrt{n} . The reason for early stages being more influential is due to the weight function $\|\mathbf{y} - \hat{\mathbf{f}}(\tau)\|_2$, which decreases during training as $\hat{\mathbf{f}}$ approaches \mathbf{y} . On the other hand, $s_{\min}(t') \in [0, 1]$ is guaranteed to be small if \mathbf{K} is nearly singular (which occurs when σ is large) for the entire training, but it can never be larger than 1. That $\overline{k}_2^*(t)$ and $s_{\min}(t')$ are both bounded from above suggests that violation of Axiom 1 due to any of them being too large is generally not a problem. However, since neither of the two quantities is bounded away from zero, poor generalization due to one, or both, of them being too small (for $s_{\min}(t')$ in combination with $t > 1/s_{\min}(t')$) poses a risk. Note, however, that as long as neither $\overline{k}_2^*(t)$ nor $s_{\min}(t')$ are too small, $\|\mathbf{k}^*(\tau)\|_2$ and $s_{\min}(\tau)$ are both allowed to temporarily be very small, without resulting in poor generalization. In summary, Proposition 1 in combination with Axiom 1, suggests that for a translational-invariant decreasing kernel generalization will be poor due to

- basically predicting the prior if
 - the bandwidth is too small too early during training ($\overline{k}_2^*(t)$ is too small) OR
 - the training time, t , is too short.

- too extreme predictions if
 - the bandwidth is too large during the entire training ($s_{\min}(t')$ is too small) AND
 - the training time, t , is too long.

The conclusions above suggest that generalization will be good if we start with a large bandwidth, which we gradually decrease toward zero during training. Thus, in the early stages of the training, the bandwidth is large, which prevents a small $\overline{k}_2^*(t)$, but, since it decreases with training time, a too small $s_{\min}(t')$ can still be avoided. The speed of the bandwidth decrease is important since the bandwidth must neither decay too fast, in which case $\overline{k}_2^*(t)$ will be too small, nor too slowly, in which case $s_{\min}(t')$ may be too small. However, before presenting our bandwidth-decreasing scheme, we will discuss the relation between bandwidth and model complexity.

3.2 Model Complexity as Function of Bandwidth

Based on Proposition 1, we argued that to obtain good generalization, one should start with a large bandwidth which is gradually decreased during training. In this section, we will arrive at the same conclusion by reasoning in terms of model complexity. The idea is to start with a simple model and let the model complexity increase during training.

Forward stagewise additive modeling is a form of boosting, where m consecutive models are used, and where model m is used to fit the residuals of model $m - 1$, i.e.

$$\begin{aligned}\hat{\mathbf{f}}'_m(\mathbf{X}) &= \arg \min_{\mathbf{f}'_m \in \mathcal{F}_m} L(\mathbf{f}'_m(\mathbf{X}), \mathbf{y} - \hat{\mathbf{f}}_{m-1}(\mathbf{X})) \\ \hat{\mathbf{f}}_m(\mathbf{X}) &= \hat{\mathbf{f}}_{m-1}(\mathbf{X}) + \hat{\mathbf{f}}'_m(\mathbf{X}),\end{aligned}$$

where \mathcal{F}_m is some class of functions and L is a loss function quantifying the discrepancy between \mathbf{f}'_m and $\mathbf{y} - \hat{\mathbf{f}}_{m-1}$.

In general, the same class, $\mathcal{F}_m = \mathcal{F}$, is used in all stages and the complexity of \mathcal{F} has to be carefully selected to obtain good performance. However, if the complexity of \mathcal{F}_m is allowed to increase with m , then simpler relations in the data will be captured first, by the simpler models, while more complex relations will be captured in later stages. Thus (ideally) each part of the data will be modeled by a model of exactly the required complexity. Furthermore, if a simple model is enough to model the data, there will be no residuals left to fit for the more complex models and the total model will not be more complex than needed.

Gradient descent is an iterative algorithm, where the update in each iteration is based on the output of the previous iteration. Thus, any iteration can be thought of as starting the training of a new model from the beginning, using the output of the previous iteration as the prior. If this interpretation is made every time the bandwidth is changed, then kernel gradient descent becomes exactly forward stagewise additive modeling, where the different models are defined by their bandwidths. Thus, if the bandwidth is updated during training in such a way that the model complexity increases during training, we would obtain exactly forward stagewise additive modeling with increasing complexity.

It is, however, not obvious how the model complexity depends on the bandwidth, but some guidance is given by Proposition 2. We first consider Equation 9, which states that the inferred function for infinite bandwidth is simply the prior plus a constant (recall that $\hat{f}(\mathbf{x}^*) = \hat{f}_\mu(\mathbf{x}^*) + \mu(\mathbf{x}^*)$), where the constant is the (shrunk) mean of the prior shifted observations. Equation 10 states the predictions for zero bandwidth. This time, the inferred function predicts the prior everywhere, except at the training observations, where the prediction is a convex combination of the observation and the prior, governed by the strength of the regularization. Arguably, a constant function is the simplest function possible, while a function that has the capacity both to perfectly model the data, and to include the prior, is the most complex function imaginable. Thus, Proposition 2 suggests that a large bandwidth corresponds to a simple model and a small bandwidth corresponds to a complex model.

Proposition 2.

Let $\overline{y}_\mu = \frac{1}{n} \sum_{i=1}^n y_{\mu,i}$ denote the mean of \mathbf{y}_μ , and let $k(\mathbf{x}, \mathbf{x}', \sigma) = k(\frac{1}{\sigma} \cdot \|\mathbf{x} - \mathbf{x}'\|_{\Theta})$ be a translational-invariant kernel such that $k(0) = 1$ and $k(\infty) = 0$.

Then, for

$$\hat{f}_\mu(\mathbf{x}^*, t, \sigma) = \mathbf{k}^*(\sigma)^\top \mathbf{K}(\sigma)^{-1} (\mathbf{I} - \exp(-t\mathbf{K}(\sigma))) \mathbf{y}_\mu$$

and

$$\hat{f}_\mu(\mathbf{x}^*, \lambda, \sigma) = \mathbf{k}^*(\sigma)^\top (\mathbf{K}(\sigma) + \lambda \mathbf{I})^{-1} \mathbf{y}_\mu,$$

$$\lim_{\sigma \rightarrow \infty} \hat{f}_\mu(\mathbf{x}^*, t, \sigma) = (1 - e^{-tn}) \cdot \bar{y}_\mu \quad (9a)$$

$$\lim_{\sigma \rightarrow \infty} \hat{f}_\mu(\mathbf{x}^*, \lambda, \sigma) = \frac{n}{n + \lambda} \cdot \bar{y}_\mu \quad (9b)$$

and

$$\lim_{\sigma \rightarrow 0} \hat{f}_\mu(\mathbf{x}^*, t, \sigma) = \begin{cases} 0 & \text{if } \mathbf{x}^* \notin \mathbf{X} \\ (1 - e^{-t}) \cdot y_{\mu,i} & \text{if } \mathbf{x}^* = \mathbf{x}_i \in \mathbf{X} \end{cases} \quad (10a)$$

$$\lim_{\sigma \rightarrow 0} \hat{f}_\mu(\mathbf{x}^*, \lambda, \sigma) = \begin{cases} 0 & \text{if } \mathbf{x}^* \notin \mathbf{X} \\ \frac{1}{1+\lambda} \cdot y_{\mu,i} & \text{if } \mathbf{x}^* = \mathbf{x}_i \in \mathbf{X}. \end{cases} \quad (10b)$$

To further characterize the relation between bandwidth and model complexity, we use the derivatives of the inferred function as a complexity measure. Intuitively, restricting the derivatives of a function restricts its complexity. This is also exactly what is done when penalizing the parameter vector, $\hat{\beta}$, in linear regression: When $\hat{f}(\mathbf{x}^*) = \mathbf{x}^{*\top} \hat{\beta}$, $\frac{\partial \hat{f}(\mathbf{x}^*)}{\partial \mathbf{x}^*} = \hat{\beta}$, and thus regression schemes such as ridge regression and lasso constrains the function complexity by restricting its derivatives. Other regression techniques where function complexity is restricted through the derivatives are Jacobian regularization (Jakubovitz and Giryes, 2018) for neural networks and smoothing splines (in the last case through the second derivative).

In Proposition 3, we relate the derivatives of $\hat{f}_\mu(\mathbf{x}^*, t)$ to the bandwidth. According to the proposition, for a fixed training time, the gradient of the inferred function is bounded by the average of the inverse bandwidth during training. We denote this average by $\overline{\sigma^{-1}}$. If the bandwidth is constant during training, $\overline{\sigma^{-1}}$ reduces to $1/\sigma$. Just as Proposition 2, Proposition 3 suggests that a model with a larger bandwidth results in a less complex inferred function, and additionally suggests that the relation between complexity and bandwidth is the multiplicative inverse.

Proposition 3.

Let $\overline{\sigma^{-1}}(t)$ denote the weighted average of the inverse bandwidth during training, with weight function $\|\mathbf{y} - \hat{\mathbf{f}}(\tau)\|_2$, i.e.,

$$\overline{\sigma^{-1}}(t) := \frac{\int_0^t \frac{1}{\sigma(\tau)} \cdot \|\mathbf{y} - \hat{\mathbf{f}}(\tau)\|_2 d\tau}{\int_0^t \|\mathbf{y} - \hat{\mathbf{f}}(\tau)\|_2 d\tau}.$$

Then, for a kernel $k(\mathbf{x}, \mathbf{x}', \sigma(\tau)) = k\left(\frac{1}{\sigma(\tau)} \cdot \|\mathbf{x} - \mathbf{x}'\|_\Theta\right)$, with bounded derivative, $|k'(u)| \leq k'_{\max} \forall u$, the KGF estimate, $\hat{f}_\mu(\mathbf{x}^*, t)$, is bounded according to

$$\left\| \frac{\partial \hat{f}_\mu(\mathbf{x}^*, t)}{\partial \mathbf{x}^*} \right\|_2 \leq \overline{\sigma^{-1}}(t) \cdot \min\left(t, \frac{1}{s_{\min}(t')}\right) \cdot \|\mathbf{y}_\mu\|_2 \cdot k'_{\max} \cdot \sqrt{n \cdot \|\Theta\|_2},$$

for the same $t' \in [0, t]$ as in Proposition 1.

Assuming the data is centered, so that $\bar{y}_\mu = 0$, we further obtain

$$\left| \hat{f}_\mu(\mathbf{x}^*, t) \right| \leq \overline{\sigma^{-1}}(t) \cdot \min\left(t, \frac{1}{s_{\min}(t')}\right) \cdot \|\mathbf{y}_\mu\|_2 \cdot k'_{\max} \cdot \sqrt{n \cdot \|\Theta\|_2} \cdot \|\mathbf{x}^* - \mathbf{x}_m\|_2, \quad (11)$$

where $\mathbf{x}_m \in \mathbf{X}$ is the observation furthest away from \mathbf{x}^* .

Remark 1: The proposition allows for σ to change during training. When σ is constant, $\overline{\sigma^{-1}}$ reduces to $1/\sigma$.

Remark 2: Equation 11 provides an alternative to Equation 8, as a function of $\overline{\sigma^{-1}}$ rather than \bar{k}_2^* .

The observation that model complexity increases as the bandwidth decreases, in combination with the forward stage-wise additive modeling interpretation, which suggests that model complexity should increase during training, thus suggests that the bandwidth should decrease during training.

3.3 Bandwidth Decreasing Scheme

We propose a bandwidth-decreasing scheme based on R^2 on training data,

$$R^2(t) = 1 - \frac{\frac{1}{n} \sum_{i=1}^n (y_i - \hat{f}_i(t))^2}{\left(\frac{1}{n} \sum_{i=1}^n (y_i - \frac{1}{n} \sum_{i=1}^n y_i)\right)^2} = 1 - \frac{\|\mathbf{y} - \hat{\mathbf{f}}(t)\|_2^2}{\|\mathbf{y} - \bar{\mathbf{y}}\|_2^2}, \quad (12)$$

where $\bar{\mathbf{y}}$ is the mean of \mathbf{y} . According to Equation 13 in Lemma 2, R^2 always increases during training, regardless of how the bandwidth is updated. However, if the kernel is kept constant, according to Equation 15, the speed of the increase decreases with training time. This means that, unless the kernel is updated, eventually the improvement of R^2 , although always positive, will be very small. Based on this observation we use the following simple update rule:

- If $\frac{\partial R^2(t)}{\partial t} = 2 \cdot \frac{\|\mathbf{y} - \hat{\mathbf{f}}(t)\|_{\mathbf{K}(t)}^2}{\|\mathbf{y} - \bar{\mathbf{y}}\|_2^2} < v_{R^2}$, decrease the bandwidth.

That is if the increase in R^2 is smaller than some threshold value, v_{R^2} , then the bandwidth is decreased until the increase is again fast enough. Otherwise, the bandwidth is kept constant.

Equation 14 has two interesting implications. First, the value of v_{R^2} might affect generalization: If $\frac{\partial R^2(t)}{\partial t}$ is allowed to be too small, $s_{\min}(\mathbf{K}(t))$ will be small enough for poor generalization due to extreme predictions to occur. Second, close to convergence, when both R^2 and $s_{\max}(\mathbf{K})$ are close to 1, it may not be possible to obtain $\frac{\partial R^2(t)}{\partial t} > v_{R^2}$ regardless how small bandwidth is chosen.

KGD with decreasing bandwidth, henceforth referred to as KGD-D, is summarized in Algorithm 1.

Lemma 2.

Let R^2 on training data be defined according to Equation 12, where $\hat{\mathbf{f}}(t)$ is the KGF estimate. Then, for a, possibly non-constant, kernel $\mathbf{K}(t)$,

$$\frac{\partial R^2(t)}{\partial t} = 2 \cdot \frac{\|\mathbf{y} - \hat{\mathbf{f}}(t)\|_{\mathbf{K}(t)}^2}{\|\mathbf{y} - \bar{\mathbf{y}}\|_2^2} \geq 0 \quad (13)$$

and

$$s_{\min}(\mathbf{K}(t)) \leq \frac{\partial R^2(t)}{\partial t} \cdot \frac{1}{2} \cdot \frac{1}{1 - R^2(t)} \leq s_{\max}(\mathbf{K}(t)), \quad (14)$$

where s_{\min} and s_{\max} denote the minimum and maximum singular values, respectively. For a constant kernel \mathbf{K} ,

$$\frac{\partial^2 R^2(t)}{\partial t^2} = -4 \cdot \frac{\|\mathbf{y} - \hat{\mathbf{f}}(t)\|_{\mathbf{K}^2}^2}{\|\mathbf{y} - \bar{\mathbf{y}}\|_2^2} \leq 0. \quad (15)$$

For KRR (and KGD/KGF), with a constant bandwidth, the hyper-parameters λ and σ have to be carefully selected to obtain a good performance. This is usually done by cross-validation, where the data is split into training and validation data, or marginal likelihood maximization, where the hyper-parameters are optimized together with the model parameters. When starting with a large bandwidth that gradually decreases to zero during training, and training until convergence, the issue of hyper-parameter selection is in some sense circumvented since many different values of σ and t are used during training. Nonetheless, instead of bandwidth and regularization, the minimum R^2 speed, v_{R^2} , which controls the decrease of σ , has to be selected. However, since R^2 is a normalized quantity, this hyper-parameter tends to generalize well across data sets. As demonstrated in Section 5, $v_{R^2} = 0.1$ usually leads to good performance.

4 Double Descent in Minimum Bandwidth

According to classical statistical knowledge, a too simple model performs poorly on both training data and in terms of generalization, since it is too simple to capture the relations in the data. A too complex model, on the other hand, performs excellently on training data but tends to generalize poorly, something that is often referred to as overfitting. However, the wisdom from double descent is that if the model is made even more complex, it may generalize well despite excellent performance on training data.

Algorithm 1 Kernel Gradient Descent with Decreasing Bandwidth, KGD-D

Input: Training data, (\mathbf{X}, \mathbf{y}) . Prediction covariates, \mathbf{X}^* . Initial bandwidth, σ_0 . Prior $\mu(\mathbf{x})$.
Minimum allowed bandwidth, σ_m . Step-size, Δt . Minimum R^2 speed, v_{R^2} . Maximum R^2 , R_{\max}^2 .

Output: Vector of predictions $[\hat{\mathbf{f}}(t)^\top, \hat{\mathbf{f}}^*(t)^\top]^\top$.

- 1: Initialize $[\hat{\mathbf{f}}(0)^\top, \hat{\mathbf{f}}^*(0)^\top]^\top = [\boldsymbol{\mu}(\mathbf{X})^\top, \boldsymbol{\mu}(\mathbf{X}^*)^\top]^\top$.
 - 2: Initialize $\sigma(0) = \sigma_0$, $\mathbf{K}(0) = \mathbf{K}(\sigma_0)$ and $\mathbf{K}^*(0) = \mathbf{K}^*(\sigma_0)$.
 - 3: **repeat**
 - 4: Calculate $R^2(t) = 1 - \frac{\|\mathbf{y} - \hat{\mathbf{f}}(t)\|_2^2}{\|\mathbf{y} - \bar{\mathbf{y}}\|_2^2}$ and $\frac{\partial R^2(t)}{\partial t} = 1 - \frac{\|\mathbf{y} - \hat{\mathbf{f}}(t)\|_{\mathbf{K}(t)}^2}{\|\mathbf{y} - \bar{\mathbf{y}}\|_2^2}$.
 - 5: **if** $\frac{\partial R^2(t)}{\partial t} < v_{R^2}$ **then**
 - 6: **repeat**
 - 7: Decrease $\sigma(t)$ and calculate $\mathbf{K}(\sigma(t))$ and $\frac{\partial R^2(t)}{\partial t}$
 - 8: **until** $\frac{\partial R^2(t)}{\partial t} \geq v_{R^2}$ **or** $\sigma(t) \leq \sigma_m$.
 - 9: Calculate $\mathbf{K}^*(\sigma(t))$.
 - 10: **end if**
 - 11: Update $[\hat{\mathbf{f}}(t)^\top, \hat{\mathbf{f}}^*(t)^\top]^\top$ according to
$$\begin{bmatrix} \hat{\mathbf{f}}(t + \Delta t) \\ \hat{\mathbf{f}}^*(t + \Delta t) \end{bmatrix} = \begin{bmatrix} \hat{\mathbf{f}}(t) \\ \hat{\mathbf{f}}^*(t) \end{bmatrix} + \Delta t \begin{bmatrix} \mathbf{K}(t) \\ \mathbf{K}^*(t) \end{bmatrix} (\mathbf{y} - \hat{\mathbf{f}}(t)).$$
 - 12: Set $t = t + \Delta t$.
 - 13: **until** $R^2(t) \geq R_{\max}^2$.
-

If we constrain the complexity of the final model by introducing a minimum allowed bandwidth, σ_m , we may, for a constant, fairly long training time (i.e. a weakly regularized model), obtain a double descent behavior in the complexity (i.e. in σ_m). This can qualitatively be seen from the bound on $|\hat{f}_\mu(\mathbf{x}^*)|$ obtained by combining Equations 8 and 11:

$$|\hat{f}_\mu(\mathbf{x}^*, t, \sigma_m)| \leq \min\left(\overline{\sigma^{-1}}(t, \sigma_m) \cdot C_1, \overline{k_2^*}(t, \sigma_m)\right) \cdot \min\left(t, \frac{1}{s_{\min}(t', \sigma_m)}\right) \cdot C_2, \quad (16)$$

where C_1 and C_2 are constants with respect to σ_m . Here, $\overline{\sigma^{-1}}$ increases with model complexity (i.e. when σ_m decreases), while $\overline{k_2^*}$ and $1/s_{\min}$ both decrease with model complexity. Thus, unless the model is very complex (i.e. if σ_m is very small), Equation 16 becomes

$$|\hat{f}_\mu(\mathbf{x}^*, t, \sigma_m)| \leq \overline{\sigma^{-1}}(t, \sigma_m) \cdot t \cdot C_1 C_2.$$

Since $\overline{\sigma^{-1}}$ increases with model complexity, for a constant t , the bound increases with model complexity from poor generalization due to basically predicting the prior (a too simple model), via good generalization due to moderate deviations from the prior, to poor generalization due to extreme predictions (overfitting). This is in line with classical statistical knowledge. However, since both $\overline{k_2^*}$ and $1/s_{\min}$ decrease with model complexity, for a very complex model (a very small σ_m), Equation 16 becomes

$$|\hat{f}_\mu(\mathbf{x}^*, t, \sigma_m)| \leq \frac{\overline{k_2^*}(t, \sigma_m)}{s_{\min}(t', \sigma_m)} \cdot C_2,$$

where $\overline{k_2^*}(t)$ and $1/s_{\min}(t')$ may be small enough to induce moderate deviations from the prior, something that implies good generalization. This is summarized in Table 1.

5 Experiments

In this section, we demonstrate KGD-D on synthetic and real data and compare it to KRR with constant bandwidth. In Section 5.1, we demonstrate on two synthetic and five real data sets how decreasing the bandwidth during training leads to improved predictive performance compared to using a constant bandwidth. In Section 5.2, we demonstrate the double descent behavior of KGD-D on one synthetic and the same five real data sets as in Section 5.1. These real data sets are presented in Table 2. In all experiments, the real data were standardized to zero mean and unit variance and split into 200 random, non-overlapping splits, each containing 100 observations (for the smaller CPU data set, we

Table 1: Conceptual sketch of how the bound on $|\hat{f}_\mu|$ from Equation 16, and thus the generalization properties, changes with model complexity, σ_m . The active elements in the minimum functions are marked in bold. In the third and fourth rows, it is not obvious which element is smaller, but this uncertainty does not affect the bounds. The constants C_1 and C_2 are omitted to improve readability. For lower model complexities, the bound on the deviation from the prior grows with model complexity, but for very complex models it starts to shrink again.

σ_m	Model Complexity	$\overline{\sigma^{-1}}$	$\overline{k_2^*}$	t	$1/s_{\min}$	Bound on $ \hat{f}_\mu $	Generalization
Large	Low	Small	Large	Mod-erate	Large	$\overline{\sigma^{-1}} \cdot t$ Small	Poor, due to basically predicting the prior
Mod-erate	Mod-erate	Mod-erate	Large	Mod-erate	Large	$\overline{\sigma^{-1}} \cdot t$ Moderate	Good, due to moderate deviations from the prior
Small	High	Large	Large	Mod-erate	Large	$\overline{\sigma^{-1}} \cdot t$ Large	Poor, due to extreme predictions
Very small	Very high	Very large	Mod-erate	Mod-erate	Mod-erate	$\overline{k_2^*}/s_{\min}$ Moderate	Good, due to moderate deviations from the prior

Table 2: Real data sets used for comparing the methods.

Data set	Size, $n \times p$
Quality of aspen tree fibres ¹	25165 \times 6
Run time of CPUs ²	8192 \times 22
Power Consumption of Tetouan City ³	52416 \times 8
Critical temperature of superconductors ⁴	21263 \times 82
Daily temperature in the U.K. in the year 2000 (Wood et al., 2017) ⁵	45568 \times 5

instead used 100 splits, 93 of them of size 82 and 7 of size 81), which in turn were split 80%/20% into training and testing data.

We consistently used the Gaussian kernel, $k(\mathbf{x}, \mathbf{x}') = \exp\left(-\frac{\|\mathbf{x}-\mathbf{x}'\|_2^2}{2\sigma^2}\right)$; in Appendix A, we also present results for four additional kernels. For KGD-D, we used $\Delta t = 0.01$, and $\sigma_0 = \max_{i,j} \|\mathbf{x}_i - \mathbf{x}_j\|_2$, where \mathbf{x}_i and \mathbf{x}_j are rows in \mathbf{X} , and, unless otherwise is stated, $v_{R^2} = 0.1$.

5.1 Kernel Gradient Descent with Decreasing Bandwidth

In this section, we compare the performance, in terms of R^2 on test data, for kernel regression with decreasing and constant bandwidth, respectively. For constant bandwidth, the bandwidth and regularization strengths were selected by generalized cross-validation, GCV, and marginal likelihood maximization, MML. For KRR with σ and λ chosen by GCV, which we abbreviate KRR-GCV, 100×100 logarithmically spaced values of the two hyper-parameters were used. When using MML, which we abbreviate KRR-MML, to mitigate the problem of convergence to a poor local optimum, 5×5 different logarithmically spaced optimization seeds were used for λ and σ .

We first demonstrate how KGD-D is able to capture different complexities in the data on two simple synthetic data sets. The first data set combines linear and sinusoidal data, and the second combines sinusoidal data of two different

¹The data set is available at <https://openmv.net/info/wood-fibres>.

²The data set is available at <https://github.com/akmand/datasets/blob/main/compactiv.csv>.

³The data set is available at <https://archive.ics.uci.edu/dataset/849/power+consumption+of+tetouan+city>.

⁴The data set is available at <https://archive.ics.uci.edu/dataset/464/superconductivity+data>.

⁵The data set is available at <https://www.maths.ed.ac.uk/~swood34>.

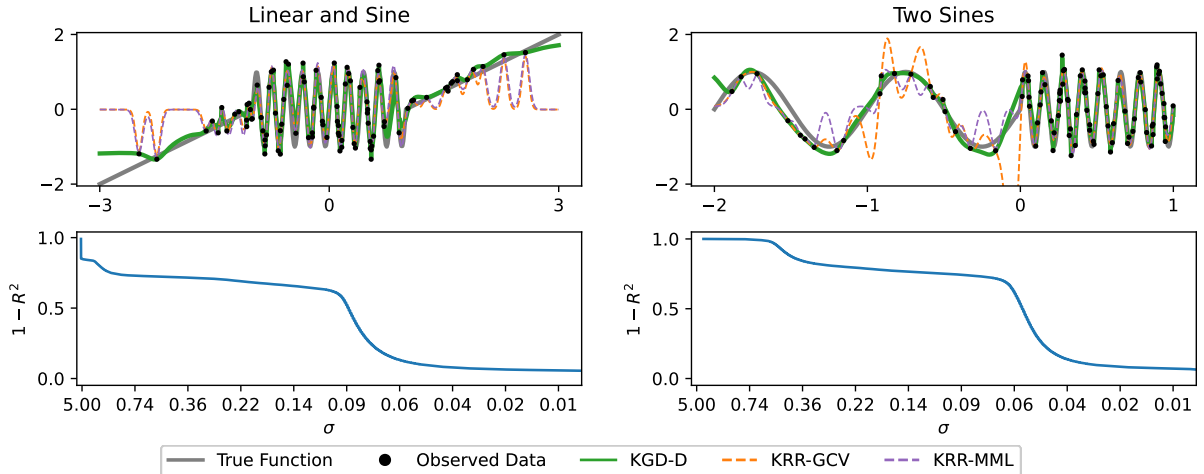


Figure 1: Top row: Inferred functions using KGD-D, KRR-GCV, and KRR-MML. When the bandwidth is allowed to change during training, all parts of the functions are captured by the model. In contrast, for a constant bandwidth, the inferred functions perform well on the high-frequency parts of the data, which has more observations, and poorly on the linear/low-frequency parts.

Bottom row: Training error for KGD-D as a function of the bandwidth, which can be used to see which bandwidths that are used to model the data. For most values of σ , the errors decrease very slowly, if at all, with distinct drops at some bandwidths, that depend on the frequencies of the sine functions.

frequencies. For the first data set, 100 observations were sampled according to

$$x \sim \mathcal{N}(0, 1^2), y = f_{1s}(x) + \mathcal{N}(0, 0.2^2),$$

$$f_{1s}(x) = \begin{cases} x - 1, & x < -1 \\ \sin(5 \cdot 2\pi x), & -1 \leq x \leq 1 \\ x + 1, & x > 1, \end{cases}$$

where $\mathcal{N}(\cdot, \cdot)$ denotes the normal distribution. For the second data set, we used stratified sampling for the x-data: 20 observations were sampled according to $x \sim \mathcal{U}(-2, 0)$ and 80 observations according to $x \sim \mathcal{U}(0, 1)$, where $\mathcal{U}(\cdot, \cdot)$ denotes the uniform distribution. The y-data were generated according to

$$y = f_{2s}(x) + \mathcal{N}(0, 0.2^2),$$

$$f_{2s}(x) = \begin{cases} \sin(2\pi x), & -2 \leq x \leq 0 \\ \sin(8 \cdot 2\pi x), & 0 < x \leq 1. \end{cases}$$

The reason for using stratified sampling is to obtain the same expected number of observations during a period for both frequencies, in this case, 10 observations per period.

The results are presented in Figure 1. In both cases, KGD-D is able to capture all parts of the function. In addition, the method combines interpolation of the training data, i.e. the inferred function goes through all observations, with accurate predictions between observations. In contrast, for constant bandwidth, the inferred functions perform well on the high-frequency parts of the data, which have more observations, and poorly on the linear/low-frequency parts. In fact, the bandwidth selected by GCV in the right column is large enough to produce a nearly singular kernel matrix, resulting in cases of extreme predictions between observations, but also small enough for the model to have a tendency to predict zero between observations.

To see which bandwidths are used to model the data, in the bottom row of the figure, we plot the training error (as $1 - R^2$) as a function of the bandwidth. We note that for most bandwidths, the error decreases very slowly, if at all, with distinct drops at some bandwidths. In the left column, a large fraction of the training data is explained already for large values of σ , i.e. when a basically linear model is used. A last drop in the error occurs when the bandwidth is approximately 0.1, which corresponds to half the wavelength of the sine wave. In the right column, there are two distinct drops in the error, the first at a bandwidth of approximately 0.5 and the second at approximately 0.0625, half the wavelengths of the two sine waves.

In Figure 2, we plot the functions by KGD-D for five different training times. Since the model complexity gradually increases during training, simpler parts of the data are modeled in earlier stages than more complex parts.

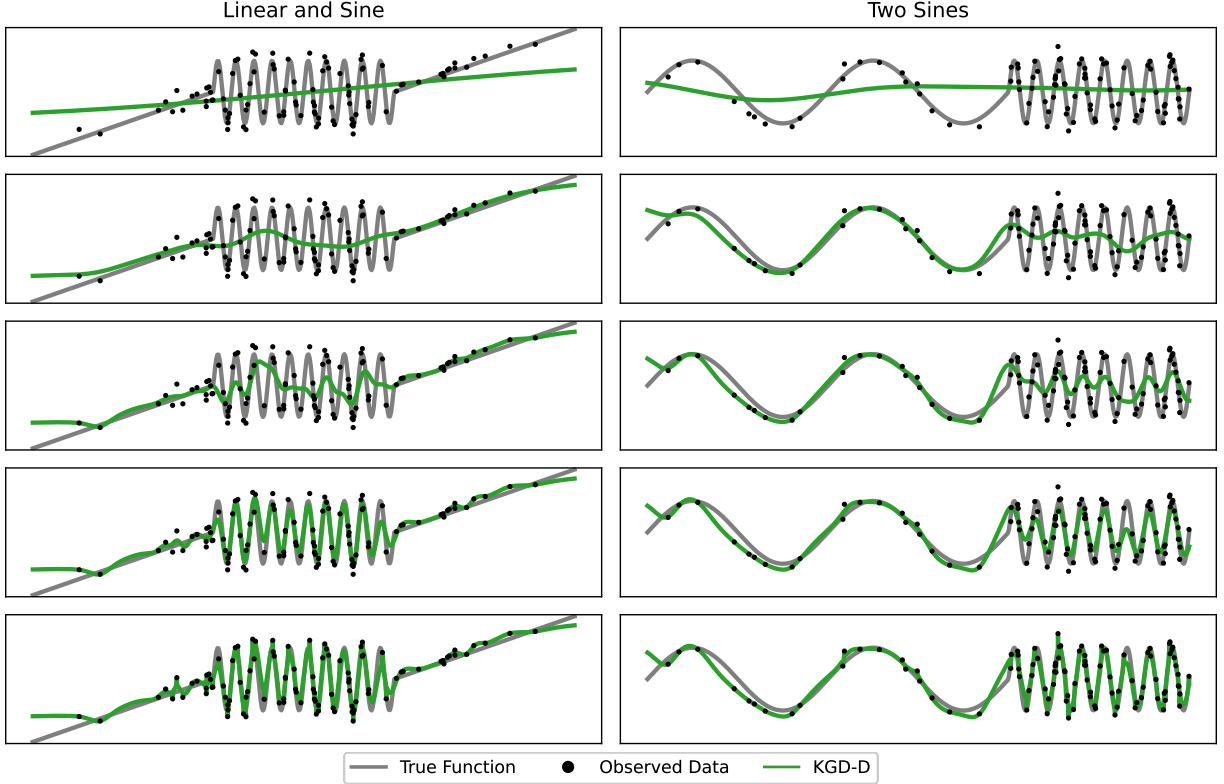


Figure 2: Inferred KGD-D functions for five different training times, where lower panels correspond to longer training times. Initially, the inferred functions are almost linear, but the complexities increase during training. Simpler parts of the data are captured earlier during training. Eventually, the models perfectly interpolate the training data.

In Table 3, we present the results for KGD-D for five different values of v_{R^2} , KRR-GCV, and KRR-MML in terms of R^2 on the test data. For $v_{R^2} = 0.1$, KGD-D performs significantly better than KRR-GCV and KRR-MML on all five data sets.

5.2 Double Descent in Minimum Bandwidth

We demonstrate double descent as a function of model complexity on the five real datasets in Table 2, and on a synthetic data set obtained by sampling 20 observations according to

$$x \sim \mathcal{U}(-1, 1), y = \sin(2\pi x) + \mathcal{N}(0, 0.2^2), \quad (17)$$

for 200 different realizations. For a fixed regularization, $\lambda = 1/t = 0.001$, KGD-D and KRR with a constant bandwidth were evaluated for 100 bandwidth values, $\{\sigma_m\}_{m=1}^{100}$. For KRR, σ_m was used during the entire training. For KGD-D, we used $v_{R^2} = 0.1$, and σ_m was used as the minimum allowed bandwidth. In Figure 3, we plot the training and test errors, as functions of σ_m , for KGD-D and KRR on the six data sets.

For large values of σ_m , both models perform poorly both in terms of training and test error. With decreasing σ_m (increasing model complexity), both the training and test errors decrease, but while the training errors always decrease, the test errors start to increase again. Approximately where the training errors become zero, there is a peak in the test errors, but while the test error for KGD-D continues to decrease with model complexity, the test error for KRR goes to $1 - R^2 = 1$, i.e. $R^2 = 0$, as σ_m goes to zero. In Figure 4, we plot the inferred functions for one realization of the synthetic data, for four indicative values of σ_m , corresponding to the four cases in Table 1. In the figure, the difference between using a constant and a decreasing bandwidth becomes apparent for small values of σ_m . For a decreasing bandwidth, since simpler models are captured in the early stages of training, a small value of σ_m , which is used only in the latter stages of the training, can be combined with good generalization. This is, however, not the case if a small bandwidth is used during the entire training, in which case we obtain a model that simply predicts the prior between the observations.

Table 3: Median and first and third quartile, over the 200 (or 100 for the CPU data) splits, of R^2 on the test data. The p-value is that of a Wilcoxon signed-rank test, testing whether the method performs better than KRR-GCV and KRR-MML, where p-values less than 0.05 are marked in bold. For $v_{R^2} = 0.1$, KGD-D performs significantly better for all data sets.

Data	Method, v_{R^2}	Test R^2	
		50%, (25%, 75%)	p-value
CPU Run Time	KGD-D, 0.02	0.800, (0.652, 0.891)	$1.6 \cdot 10^{-7}$
	KGD-D, 0.05	0.793, (0.620, 0.888)	$5.6 \cdot 10^{-6}$
	KGD-D, 0.1	0.769, (0.579, 0.867)	0.0038
	KGD-D, 0.2	0.695, (0.533, 0.836)	0.18
	KGD-D, 0.5	0.640, (0.407, 0.799)	0.89
	KRR-GCV	0.693, (0.411, 0.855)	—
	KRR-MML	0.493, (0.126, 0.678)	—
Tetouan Power Consumption	KGD-D, 0.02	0.615, (0.470, 0.721)	0.92
	KGD-D, 0.05	0.654, (0.523, 0.747)	0.00025
	KGD-D, 0.1	0.668, (0.549, 0.759)	$5.4 \cdot 10^{-9}$
	KGD-D, 0.2	0.660, (0.554, 0.746)	$7.4 \cdot 10^{-7}$
	KGD-D, 0.5	0.613, (0.489, 0.694)	0.98
	KRR-GCV	0.608, (0.448, 0.736)	—
	KRR-MML	0.527, (0.402, 0.632)	—
Superconductor Critical Temperature	KGD-D, 0.02	0.645, (0.516, 0.737)	1
	KGD-D, 0.05	0.671, (0.560, 0.763)	0.032
	KGD-D, 0.1	0.675, (0.569, 0.760)	$1.8 \cdot 10^{-5}$
	KGD-D, 0.2	0.669, (0.564, 0.745)	0.00033
	KGD-D, 0.5	0.617, (0.518, 0.694)	1
	KRR-GCV	0.645, (0.540, 0.733)	—
	KRR-MML	0.566, (0.461, 0.643)	—
U.K. Temperature	KGD-D, 0.02	0.459, (0.311, 0.582)	1
	KGD-D, 0.05	0.522, (0.396, 0.625)	0.82
	KGD-D, 0.1	0.545, (0.439, 0.643)	0.0048
	KGD-D, 0.2	0.546, (0.440, 0.634)	0.00063
	KGD-D, 0.5	0.491, (0.392, 0.580)	1
	KRR-GCV	0.521, (0.402, 0.611)	—
	KRR-MML	0.457, (0.365, 0.526)	—
Aspen Fibres	KGD-D, 0.02	0.359, (0.0441, 0.602)	0.96
	KGD-D, 0.05	0.431, (0.221, 0.648)	0.2
	KGD-D, 0.1	0.497, (0.324, 0.664)	0.0006
	KGD-D, 0.2	0.542, (0.370, 0.662)	$1.3 \cdot 10^{-8}$
	KGD-D, 0.5	0.544, (0.408, 0.671)	$7.8 \cdot 10^{-15}$
	KRR-GCV	0.448, (0.194, 0.593)	—
	KRR-MML	0.260, (-0.138, 0.485)	—

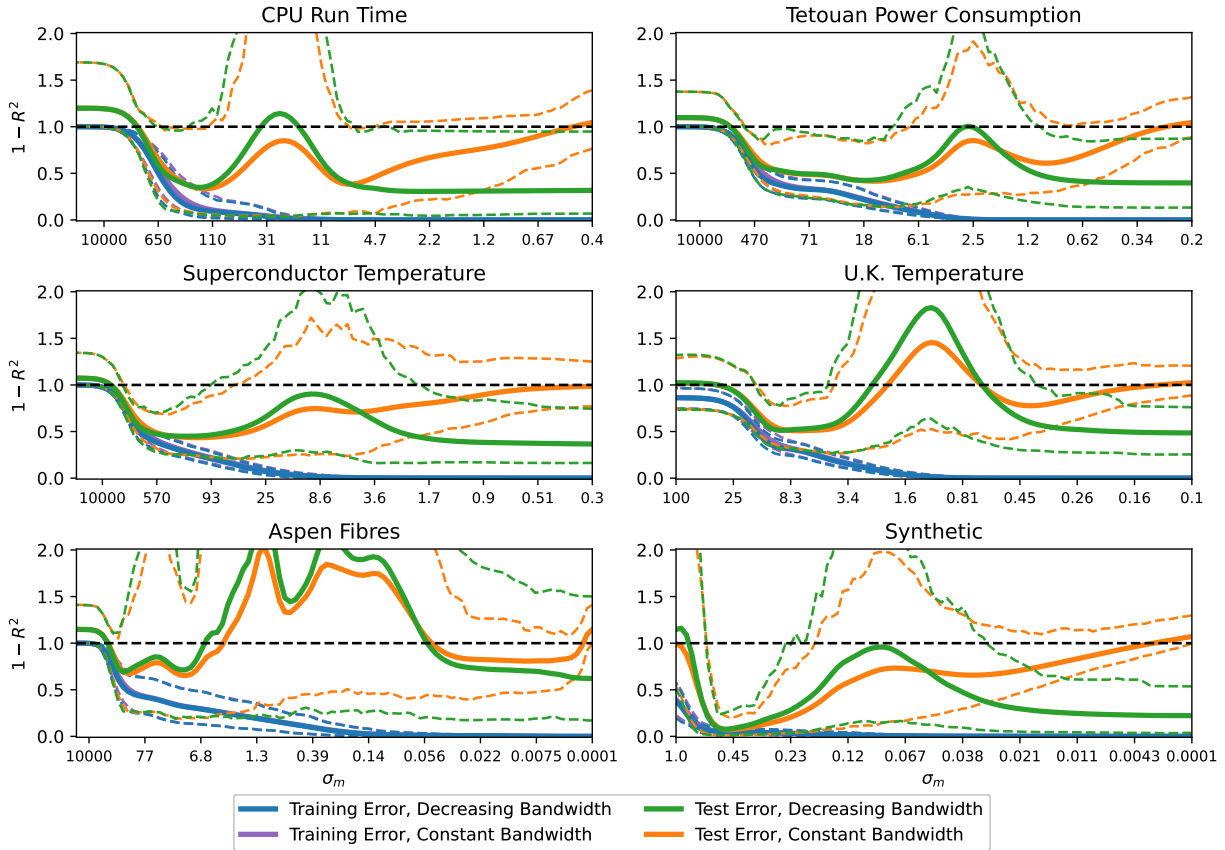


Figure 3: Training and test errors (as $1 - R^2$) as functions of model complexity (in terms of σ_m), for kernel regression with constant and decreasing bandwidths. The plots show the means, together with the 90% prediction intervals. For simple models, both the training and test errors are large, but they all decrease with increasing model complexity. While the training errors decrease toward zero, the test errors start to increase again as the models become even more complex. When using a decreasing bandwidth, a second descent in the error results in good generalization for very complex models, something that is not the case for the constant bandwidth model.

6 Conclusions

We generalized kernel gradient descent to non-constant kernels and addressed the implications this has on generalization. Based on our theoretical analysis, we proposed an update scheme for the bandwidth of the kernel during training, obtaining a method that combines zero training error with good generalization. We also related the bandwidth to model complexity and theoretically addressed the phenomenon of double descent as a function of model complexity. On real and synthetic data, we demonstrated that decreasing the bandwidth during training leads to superior predictive performance, and verified our theoretical findings about double descent.

Kernel regression with non-constant kernels opens up both for better performance on complicated data sets and for a better understanding of generalization as a function of model complexity. An interesting future line of research would be to try to apply our findings to other iteratively trained non-linear regression models. The obvious example would be neural networks, which are also known for combining zero training error with good generalization, and for displaying a double descent behavior.

Code is available at https://github.com/allerbo/non_constant_kgd.

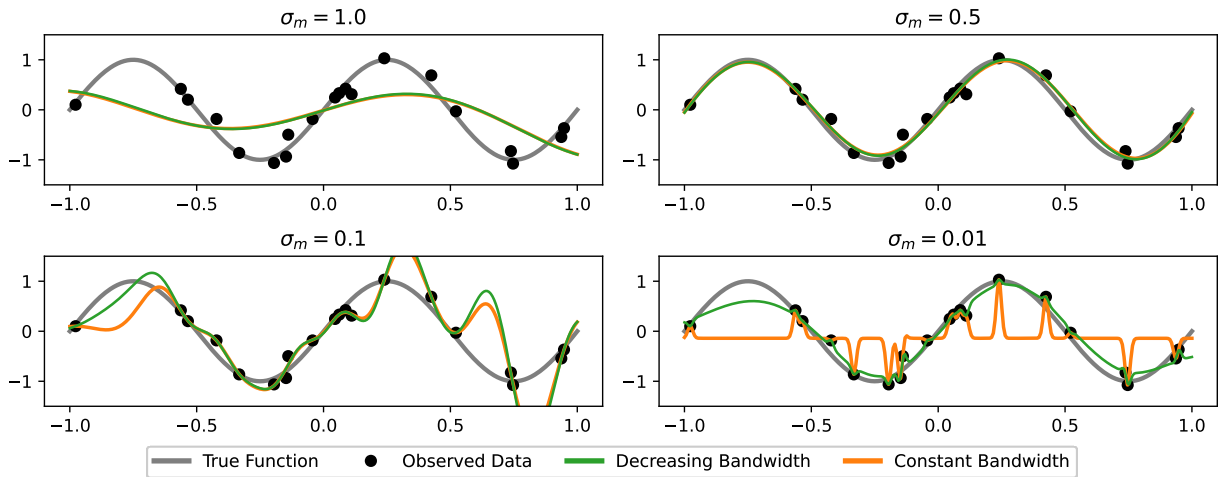


Figure 4: Inferred models for the data generated according to Equation 17, for different model complexities, corresponding to the four cases in Table 1. For $\sigma_m = 1$, the models are too simple and perform badly on both training and test data. For $\sigma_m = 0.5$, the models do well on both training and test data. For $\sigma_m = 0.1$, the models perfectly explain the training data but tend to exhibit extreme predictions between observations. For $\sigma_m = 0.01$, both models perfectly explain the training data, but in contrast to the decreasing bandwidth model, the constant bandwidth model tends to generalize poorly.

References

- Advani, M. S., Saxe, A. M., and Sompolinsky, H. (2020). High-dimensional dynamics of generalization error in neural networks. *Neural Networks*, 132:428–446.
- Ali, A., Kolter, J. Z., and Tibshirani, R. J. (2019). A continuous-time view of early stopping for least squares regression. In *The 22nd International Conference on Artificial Intelligence and Statistics*, pages 1370–1378. PMLR.
- Ali, M., Prasad, R., Xiang, Y., and Yaseen, Z. M. (2020). Complete ensemble empirical mode decomposition hybridized with random forest and kernel ridge regression model for monthly rainfall forecasts. *Journal of Hydrology*, 584:124647.
- Allerbo, O. (2023). Fast robust kernel regression through sign gradient descent with early stopping. *arXiv preprint arXiv:2306.16838*.
- Allerbo, O., Jonasson, J., and Jörnsten, R. (2023). Elastic gradient descent, an iterative optimization method approximating the solution paths of the elastic net. *Journal of Machine Learning Research*, 24(277):1–53.
- Bartlett, P. L., Montanari, A., and Rakhlin, A. (2021). Deep learning: a statistical viewpoint. *Acta Numerica*, 30:87–201.
- Belkin, M., Hsu, D., Ma, S., and Mandal, S. (2019). Reconciling modern machine-learning practice and the classical bias–variance trade-off. *Proceedings of the National Academy of Sciences*, 116(32):15849–15854.
- Belkin, M., Ma, S., and Mandal, S. (2018). To understand deep learning we need to understand kernel learning. In *International Conference on Machine Learning*, pages 541–549. PMLR.
- Chen, H. and Leclair, J. (2021). Optimizing etching process recipe based on kernel ridge regression. *Journal of Manufacturing Processes*, 61:454–460.
- Chen, Z., Hu, J., Qiu, X., and Jiang, W. (2022). Kernel ridge regression-based tv regularization for motion correction of dynamic MRI. *Signal Processing*, 197:108559.
- Fan, P., Deng, R., Qiu, J., Zhao, Z., and Wu, S. (2021). Well logging curve reconstruction based on kernel ridge regression. *Arabian Journal of Geosciences*, 14(16):1–10.
- Friedman, J. and Popescu, B. E. (2004). Gradient directed regularization. *Unpublished manuscript*.
- Jacot, A., Gabriel, F., and Hongler, C. (2018). Neural tangent kernel: Convergence and generalization in neural networks. *Advances in Neural Information Processing Systems*, 31.
- Jakubovitz, D. and Giryes, R. (2018). Improving DNN robustness to adversarial attacks using Jacobian regularization. In *Proceedings of the European Conference on Computer Vision (ECCV)*, pages 514–529.
- Kalimeris, D., Kaplun, G., Nakkiran, P., Edelman, B., Yang, T., Barak, B., and Zhang, H. (2019). Sgd on neural networks learns functions of increasing complexity. *Advances in Neural Information Processing Systems*, 32.
- Krige, D. G. (1951). A statistical approach to some basic mine valuation problems on the Witwatersrand. *Journal of the Southern African Institute of Mining and Metallurgy*, 52(6):119–139.
- Le, Y., Jin, S., Zhang, H., Shi, W., and Yao, H. (2021). Fingerprinting indoor positioning method based on kernel ridge regression with feature reduction. *Wireless Communications and Mobile Computing*, 2021.
- Ma, S. and Belkin, M. (2017). Diving into the shallows: a computational perspective on large-scale shallow learning. *Advances in Neural Information Processing Systems*, 30.
- Mason, L., Baxter, J., Bartlett, P., and Frean, M. (1999). Boosting algorithms as gradient descent. *Advances in Neural Information Processing Systems*, 12.
- Matheron, G. (1963). Principles of geostatistics. *Economic Geology*, 58(8):1246–1266.
- Raskutti, G., Wainwright, M. J., and Yu, B. (2014). Early stopping and non-parametric regression: an optimal data-dependent stopping rule. *Journal of Machine Learning Research*, 15(1):335–366.
- Rugh, W. J. (1996). *Linear System Theory*. Prentice-Hall, Inc.
- Safari, M. J. S. and Rahimzadeh Arashloo, S. (2021). Kernel ridge regression model for sediment transport in open channel flow. *Neural Computing and Applications*, 33(17):11255–11271.
- Shahsavari, A., Jamei, M., and Karbasi, M. (2021). Experimental evaluation and development of predictive models for rheological behavior of aqueous Fe₃O₄ ferrofluid in the presence of an external magnetic field by introducing a novel grid optimization based-Kernel ridge regression supported by sensitivity analysis. *Powder Technology*, 393:1–11.

- Singh Alvarado, J., Goffinet, J., Michael, V., Liberti, W., Hatfield, J., Gardner, T., Pearson, J., and Mooney, R. (2021). Neural dynamics underlying birdsong practice and performance. *Nature*, 599(7886):635–639.
- Wood, S. N., Li, Z., Shaddick, G., and Augustin, N. H. (2017). Generalized additive models for gigadata: Modeling the UK black smoke network daily data. *Journal of the American Statistical Association*, 112(519):1199–1210.
- Wu, Y., Prezhdo, N., and Chu, W. (2021). Increasing efficiency of nonadiabatic molecular dynamics by hamiltonian interpolation with kernel ridge regression. *The Journal of Physical Chemistry A*, 125(41):9191–9200.
- Yao, Y., Rosasco, L., and Caponnetto, A. (2007). On early stopping in gradient descent learning. *Constructive Approximation*, 26(2):289–315.
- Zahrt, A. F., Henle, J. J., Rose, B. T., Wang, Y., Darrow, W. T., and Denmark, S. E. (2019). Prediction of higher-selectivity catalysts by computer-driven workflow and machine learning. *Science*, 363(6424):eaau5631.
- Zhang, C., Bengio, S., Hardt, M., Recht, B., and Vinyals, O. (2021). Understanding deep learning (still) requires rethinking generalization. *Communications of the ACM*, 64(3):107–115.

Table 4: Additional kernels used

Name	Equation
Matérn, $\nu = \frac{1}{2}$ (Laplace)	$\exp\left(-\frac{\ \mathbf{x}-\mathbf{x}'\ _2}{\sigma}\right)$
Matérn, $\nu = \frac{3}{2}$	$\left(1 + \frac{\sqrt{3}\cdot\ \mathbf{x}-\mathbf{x}'\ _2}{\sigma}\right) \cdot \exp\left(-\frac{\sqrt{3}\cdot\ \mathbf{x}-\mathbf{x}'\ _2}{\sigma}\right)$
Matérn, $\nu = \frac{5}{2}$	$\left(1 + \frac{\sqrt{5}\cdot\ \mathbf{x}-\mathbf{x}'\ _2}{\sigma} + \frac{5\cdot\ \mathbf{x}-\mathbf{x}'\ _2^2}{3\cdot\sigma^2}\right) \cdot \exp\left(-\frac{\sqrt{5}\cdot\ \mathbf{x}-\mathbf{x}'\ _2}{\sigma}\right)$
Cauchy	$\left(1 + \frac{\ \mathbf{x}-\mathbf{x}'\ _2^2}{\sigma^2}\right)^{-1}$

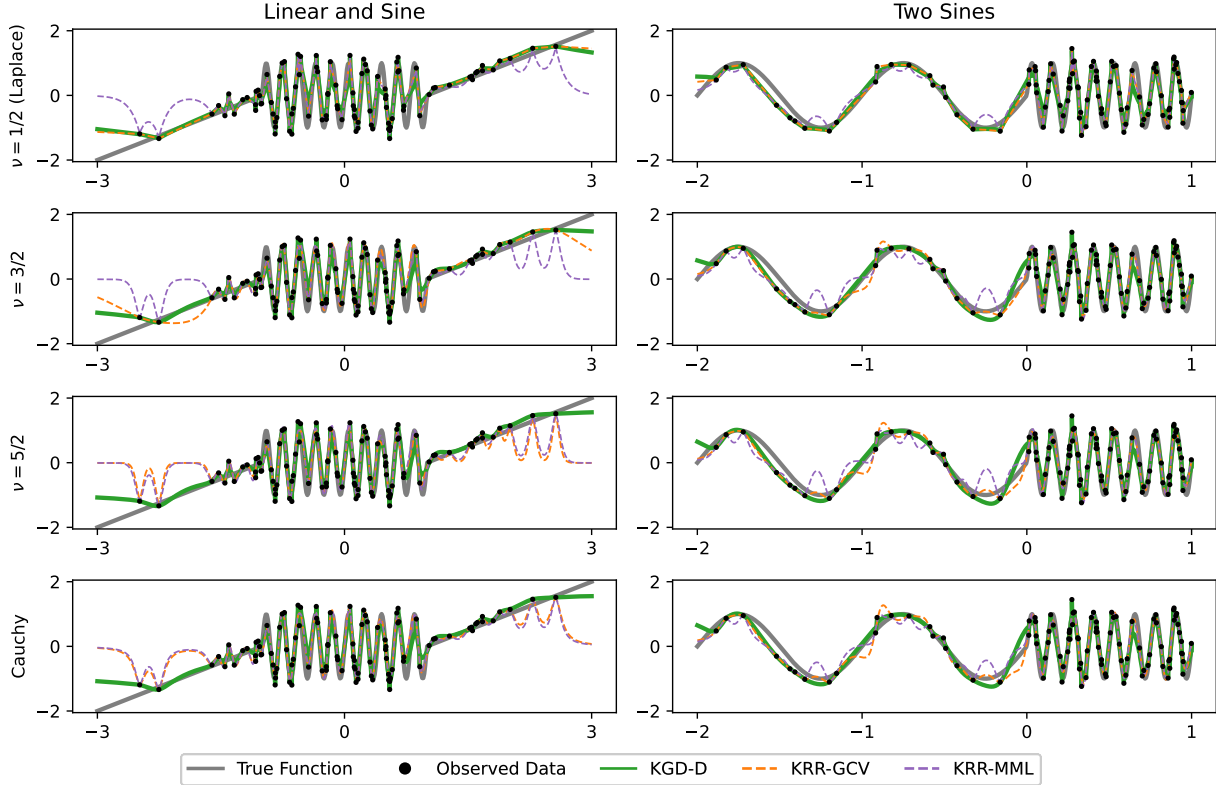


Figure 5: Inferred functions on the same data as in Figure 1, for the four kernels in Table 4. Regardless of the kernel, the functions tend to be similar, with one exception: For small values of ν , which corresponds to lower smoothness of the kernel (in terms of differentiability), constant bandwidth functions tend to linearly interpolate the data.

A Additional Experiments

In this section, we repeat the experiments of Section 5 for the four kernels in Table 4. The analogues of Figure 1 and Table 3 are presented in Figure 5 and Tables 5 and 6. The results confirm those of Section 5.1 with one exception: In Table 5, KRR-GCV tends to outperform KGD-D on multiple data sets. This can probably be attributed to the fact that for $\nu = 1/2$ (the Laplace kernel), all derivatives of the kernel, and thus of the inferred function, are discontinuous, while for $\nu = 3/2$ the same holds for all derivatives of higher order than one. As can be seen in Figure 5, for KRR-GCV, these two kernels, especially $\nu = 1/2$, tend to perform linear interpolation between the observations, which reduces the impact of the constant bandwidth. We also note in Table 5 that the advantage of KRR-GCV compared to KGD-D is larger for $\nu = 1/2$ than for $\nu = 3/2$, which supports this hypothesis. However, with the exception of the Aspen Fibres data, KGD-D with the Gaussian kernel always outperforms KRR-GCV with the Laplace kernel.

The analogues of Figures 3 and Table 4 are presented in Figure 6 and 7. Again, the results confirm those of Section 5.1 with the exception of the Laplace kernel, which tends to linearly interpolate the data. Thus, there are no extreme predictions between observations and no peaks in the test errors.

Table 5: Median and first and third quartile, over the 200 (or 100 for the CPU data) splits, of R^2 on the test data. The p-value is that of a Wilcoxon signed-rank test, testing whether the method performs better than KRR-GCV and KRR-MML, where p-values less than 0.05 are marked in bold.

Data	Method, v_{R^2}	Test $R^2, \nu = 1/2$ (Laplace)			Test $R^2, \nu = 3/2$		
		50%,	(25%, 75%)	p-value	50%,	(25%, 75%)	p-value
CPU Run Time	KGD-D, 0.02	0.696,	(0.496, 0.813)	0.22	0.794,	(0.620, 0.879)	0.00076
	KGD-D, 0.05	0.678,	(0.484, 0.798)	1	0.765,	(0.597, 0.870)	0.27
	KGD-D, 0.1	0.659,	(0.469, 0.789)	1	0.735,	(0.540, 0.845)	0.98
	KGD-D, 0.2	0.628,	(0.435, 0.767)	1	0.690,	(0.471, 0.815)	1
	KGD-D, 0.5	0.543,	(0.335, 0.744)	1	0.614,	(0.401, 0.781)	1
	KRR-GCV	0.722,	(0.478, 0.827)	—	0.759,	(0.572, 0.862)	—
	KRR-MML	0.455,	(0.189, 0.656)	—	0.502,	(0.168, 0.680)	—
Tetouan Power Consumption	KGD-D, 0.02	0.652,	(0.549, 0.739)	0.97	0.656,	(0.523, 0.749)	0.95
	KGD-D, 0.05	0.644,	(0.534, 0.733)	1	0.666,	(0.550, 0.751)	0.063
	KGD-D, 0.1	0.636,	(0.525, 0.723)	1	0.667,	(0.553, 0.750)	0.046
	KGD-D, 0.2	0.614,	(0.514, 0.699)	1	0.640,	(0.539, 0.736)	0.94
	KGD-D, 0.5	0.554,	(0.452, 0.627)	1	0.598,	(0.481, 0.672)	1
	KRR-GCV	0.652,	(0.542, 0.742)	—	0.650,	(0.513, 0.741)	—
	KRR-MML	0.497,	(0.407, 0.587)	—	0.521,	(0.415, 0.620)	—
Superconductor Critical Temperature	KGD-D, 0.02	0.679,	(0.576, 0.762)	$1.3 \cdot 10^{-9}$	0.665,	(0.551, 0.765)	0.94
	KGD-D, 0.05	0.674,	(0.572, 0.757)	$1.1 \cdot 10^{-7}$	0.676,	(0.570, 0.773)	0.042
	KGD-D, 0.1	0.666,	(0.561, 0.752)	0.0024	0.682,	(0.573, 0.763)	0.0027
	KGD-D, 0.2	0.647,	(0.551, 0.738)	0.95	0.667,	(0.561, 0.745)	0.44
	KGD-D, 0.5	0.590,	(0.502, 0.671)	1	0.608,	(0.519, 0.696)	1
	KRR-GCV	0.664,	(0.552, 0.746)	—	0.654,	(0.548, 0.757)	—
	KRR-MML	0.562,	(0.452, 0.636)	—	0.568,	(0.462, 0.650)	—
U.K. Temperature	KGD-D, 0.02	0.527,	(0.417, 0.635)	0.0014	0.522,	(0.412, 0.626)	1
	KGD-D, 0.05	0.527,	(0.418, 0.634)	0.15	0.534,	(0.429, 0.639)	0.55
	KGD-D, 0.1	0.514,	(0.403, 0.618)	1	0.546,	(0.440, 0.641)	0.11
	KGD-D, 0.2	0.502,	(0.387, 0.586)	1	0.535,	(0.427, 0.635)	0.93
	KGD-D, 0.5	0.425,	(0.324, 0.504)	1	0.476,	(0.364, 0.551)	1
	KRR-GCV	0.526,	(0.425, 0.627)	—	0.533,	(0.435, 0.643)	—
	KRR-MML	0.366,	(0.277, 0.427)	—	0.416,	(0.327, 0.488)	—
Aspen Fibres	KGD-D, 0.02	0.493,	(0.340, 0.649)	1	0.435,	(0.203, 0.631)	1
	KGD-D, 0.05	0.520,	(0.369, 0.658)	1	0.465,	(0.292, 0.641)	0.99
	KGD-D, 0.1	0.522,	(0.386, 0.666)	0.95	0.525,	(0.352, 0.651)	0.58
	KGD-D, 0.2	0.534,	(0.397, 0.667)	0.95	0.548,	(0.369, 0.675)	0.004
	KGD-D, 0.5	0.534,	(0.415, 0.664)	0.95	0.552,	(0.423, 0.673)	$1.3 \cdot 10^{-5}$
	KRR-GCV	0.558,	(0.390, 0.680)	—	0.514,	(0.320, 0.657)	—
	KRR-MML	0.462,	(0.237, 0.629)	—	0.264,	(0.0314, 0.524)	—

B Proofs

Proof of Lemma 1.

$$\begin{aligned}
\left| \mathbf{k}^{*\top} (\mathbf{I} - \exp(-t\mathbf{K})) \mathbf{K}^{-1} \mathbf{y}_\mu \right| &\leq \|\mathbf{k}^*\|_2 \cdot \|(\mathbf{I} - \exp(-t\mathbf{K})) \mathbf{K}^{-1}\|_2 \cdot \|\mathbf{y}_\mu\|_2 \\
&= \|\mathbf{k}^*\|_2 \cdot \frac{1 - e^{-t \cdot s_{\min}}}{s_{\min}} \cdot \|\mathbf{y}_\mu\|_2 \\
&\leq \|\mathbf{k}^*\|_2 \cdot \max\left(t, \frac{1}{s_{\min}}\right) \cdot \|\mathbf{y}_\mu\|_2,
\end{aligned}$$

Table 6: Median and first and third quartile, over the 200 (or 100 for the CPU data) splits, of R^2 on the test data. The p-value is that of a Wilcoxon signed-rank test, testing whether the method performs better than KRR-GCV and KRR-MML, where p-values less than 0.05 are marked in bold. Except for the CPU data, for which only 100 splits were used, KGD-D performs significantly better for all data sets for $v_{R^2} = 0.1$.

Data	Method, v_{R^2}	Test R^2 , $\nu = 5/2$		Test R^2 , Cauchy	
		50%, (25%, 75%)	p-value	50%, (25%, 75%)	p-value
CPU Run Time	KGD-D, 0.02	0.809, (0.645, 0.882)	$3 \cdot 10^{-5}$	0.798, (0.633, 0.883)	0.00032
	KGD-D, 0.05	0.796, (0.597, 0.879)	0.0028	0.778, (0.594, 0.880)	0.028
	KGD-D, 0.1	0.765, (0.559, 0.862)	0.18	0.745, (0.543, 0.853)	0.58
	KGD-D, 0.2	0.697, (0.496, 0.822)	0.88	0.693, (0.479, 0.818)	0.99
	KGD-D, 0.5	0.631, (0.406, 0.779)	1	0.614, (0.407, 0.779)	1
	KRR-GCV	0.732, (0.509, 0.851)	—	0.743, (0.525, 0.845)	—
	KRR-MML	0.498, (0.161, 0.688)	—	0.491, (0.209, 0.682)	—
Tetouan Power Consumption	KGD-D, 0.02	0.644, (0.507, 0.733)	0.95	0.646, (0.503, 0.733)	0.55
	KGD-D, 0.05	0.665, (0.545, 0.753)	0.0082	0.666, (0.550, 0.756)	0.00011
	KGD-D, 0.1	0.666, (0.555, 0.756)	0.00013	0.666, (0.552, 0.753)	$4.1 \cdot 10^{-6}$
	KGD-D, 0.2	0.653, (0.545, 0.742)	0.099	0.643, (0.538, 0.739)	0.14
	KGD-D, 0.5	0.605, (0.483, 0.678)	1	0.594, (0.472, 0.668)	1
	KRR-GCV	0.635, (0.489, 0.737)	—	0.628, (0.469, 0.743)	—
	KRR-MML	0.526, (0.415, 0.625)	—	0.509, (0.414, 0.609)	—
Superconductor Critical Temperature	KGD-D, 0.02	0.657, (0.538, 0.757)	0.99	0.661, (0.543, 0.761)	0.98
	KGD-D, 0.05	0.672, (0.568, 0.770)	0.075	0.676, (0.570, 0.773)	0.071
	KGD-D, 0.1	0.681, (0.570, 0.764)	0.0012	0.682, (0.572, 0.764)	0.005
	KGD-D, 0.2	0.669, (0.561, 0.743)	0.13	0.667, (0.561, 0.745)	0.34
	KGD-D, 0.5	0.612, (0.517, 0.696)	1	0.604, (0.519, 0.692)	1
	KRR-GCV	0.648, (0.554, 0.752)	—	0.648, (0.547, 0.754)	—
	KRR-MML	0.569, (0.461, 0.645)	—	0.561, (0.453, 0.640)	—
U.K. Temperature	KGD-D, 0.02	0.501, (0.382, 0.609)	1	0.504, (0.387, 0.609)	1
	KGD-D, 0.05	0.530, (0.423, 0.638)	0.43	0.534, (0.433, 0.638)	0.053
	KGD-D, 0.1	0.546, (0.447, 0.643)	0.0015	0.553, (0.452, 0.643)	$1 \cdot 10^{-5}$
	KGD-D, 0.2	0.548, (0.437, 0.637)	0.043	0.546, (0.434, 0.640)	0.017
	KGD-D, 0.5	0.487, (0.378, 0.561)	1	0.475, (0.363, 0.554)	1
	KRR-GCV	0.539, (0.422, 0.630)	—	0.535, (0.421, 0.634)	—
	KRR-MML	0.431, (0.341, 0.498)	—	0.391, (0.310, 0.471)	—
Aspen Fibres	KGD-D, 0.02	0.417, (0.167, 0.605)	1	0.410, (0.198, 0.610)	0.84
	KGD-D, 0.05	0.453, (0.266, 0.648)	0.67	0.468, (0.266, 0.638)	0.2
	KGD-D, 0.1	0.505, (0.334, 0.648)	0.064	0.515, (0.335, 0.648)	0.0033
	KGD-D, 0.2	0.550, (0.372, 0.664)	$8.8 \cdot 10^{-5}$	0.543, (0.375, 0.665)	$4.7 \cdot 10^{-7}$
	KGD-D, 0.5	0.552, (0.405, 0.670)	$3.7 \cdot 10^{-9}$	0.549, (0.416, 0.669)	$7.8 \cdot 10^{-11}$
	KRR-GCV	0.473, (0.294, 0.629)	—	0.469, (0.272, 0.626)	—
	KRR-MML	0.303, (-0.0394, 0.511)	—	0.268, (-0.0665, 0.468)	—

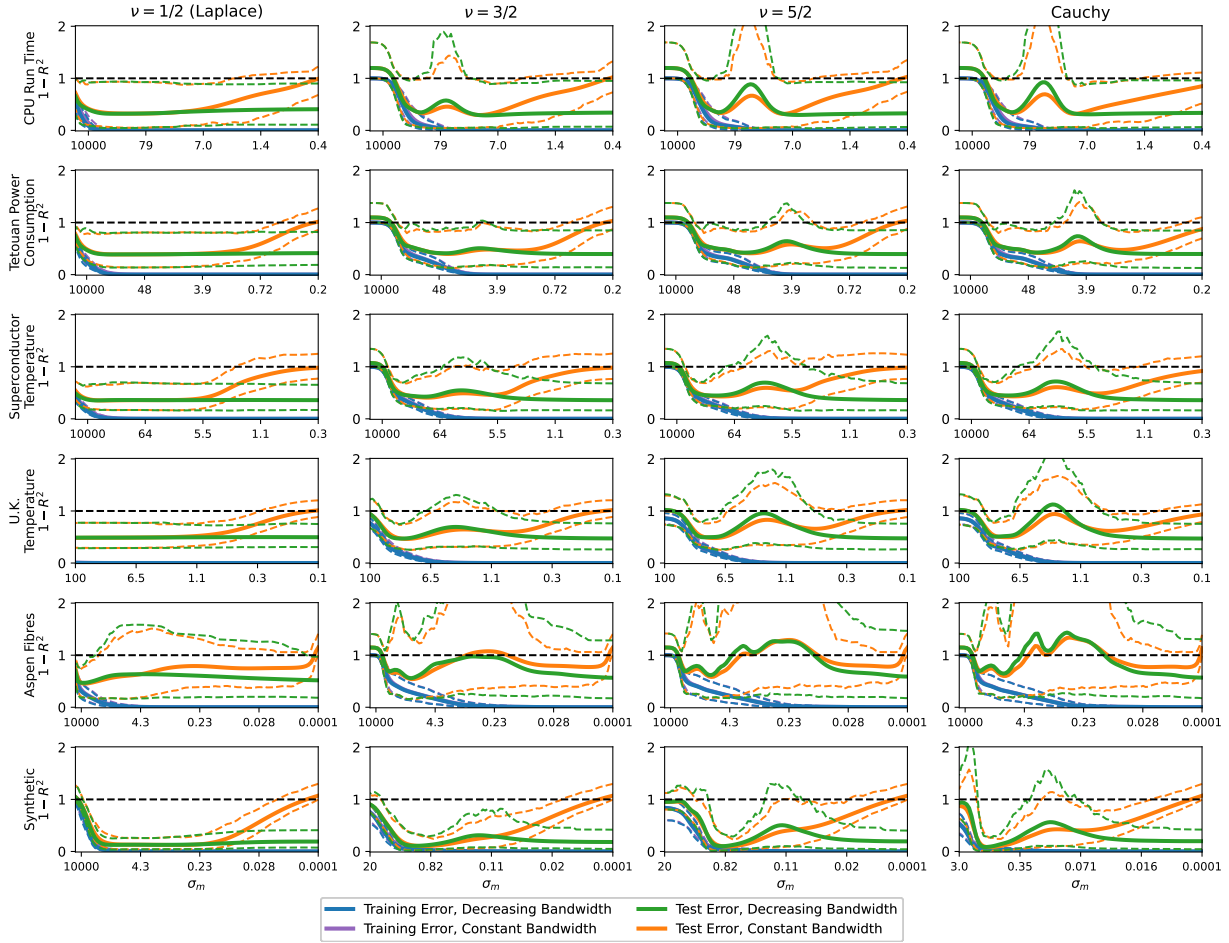


Figure 6: Training and test errors (as $1 - R^2$) as functions of model complexity (as in terms of σ_m), for kernel regression with constant and decreasing bandwidths. The plots show the means, together with the 90% prediction intervals. Except for $\nu = 1/2$, for which the kernel and inferred functions tend to linearly interpolate the data, the results agree with those of Figure 3.

where in the last equality we used $\|\mathbf{A}\|_2 = s_{\max}(\mathbf{A})$ and the fact that $\frac{1-e^{-t \cdot s}}{s}$ is a decreasing function in s , and in the last inequality we used Lemma 3.

$$\begin{aligned} \|\mathbf{k}^{*\top}(\mathbf{K} + \lambda\mathbf{I})^{-1}\mathbf{y}_\mu\| &\leq \|\mathbf{k}^*\|_2 \cdot \|(\mathbf{K} + \lambda\mathbf{I})^{-1}\|_2 \cdot \|\mathbf{y}_\mu\|_2 = \|\mathbf{k}^*\|_2 \cdot \frac{1}{s_{\min} + \lambda} \cdot \|\mathbf{y}_\mu\|_2 \\ &\leq \|\mathbf{k}^*\|_2 \cdot \max\left(\frac{1}{\lambda}, \frac{1}{s_{\min}}\right) \cdot \|\mathbf{y}_\mu\|_2, \end{aligned}$$

where in the last equality we used $\|\mathbf{A}\|_2 = s_{\max}(\mathbf{A})$ and $s_{\max}(\mathbf{A}) = 1/s_{\min}(\mathbf{A}^{-1})$, and in the last inequality we used $\lambda, s_{\min} \geq 0$. \square

Lemma 3.

For $s, t > 0$,

$$\frac{1 - e^{-ts}}{s} \leq \min\left(t, \frac{1}{s}\right).$$

Proof.

That

$$\frac{1 - e^{-ts}}{s} \leq \frac{1}{s}$$

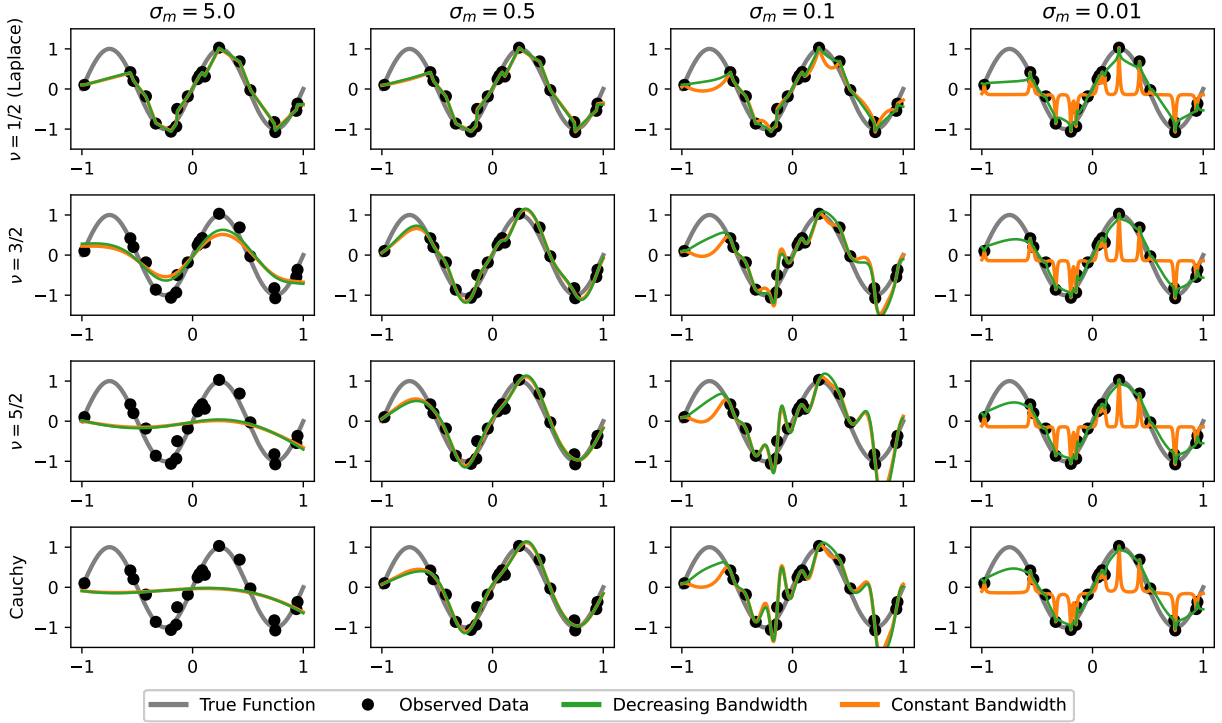


Figure 7: Inferred functions on the same data as in Figure 1, for the four kernels in Table 4. Regardless of the kernel, the functions tend to be similar, with one exception: For $\nu = 1/2$, when the kernel and inferred function have non-continuous derivatives, for large bandwidths, the constant bandwidth functions tend to linearly interpolate the data.

follows immediately from $e^{-ts} \in [0, 1]$ for $s, t \geq 0$.

To show that

$$\frac{1 - e^{-ts}}{s} \leq t,$$

we first show that $\frac{1 - e^{-ts}}{s}$ is a decreasing function in s :

$$\frac{\partial}{\partial s} \left(\frac{1 - e^{-ts}}{s} \right) = \frac{e^{-st}(st - e^{st} + 1)}{s^2}.$$

The derivative is non-positive if, for $x = ts$, $x - e^x + 1 \leq 0$. We calculate the maximum by setting the derivative to zero,

$$0 = \frac{\partial}{\partial x} (x - e^x + 1) = 1 - e^x \implies x = 0 \implies \max_x (x - e^x + 1) = 0 - e^0 + 1 = 0.$$

Thus $\frac{1 - e^{-ts}}{s}$ is a decreasing function in s , and obtains its maximum in the smallest allowed value of s , which is $s = 0$:

$$\lim_{s \rightarrow 0} \left(\frac{1 - e^{-ts}}{s} \right) = \lim_{s \rightarrow 0} \left(\frac{1 - 1 + ts + \mathcal{O}(s^2)}{s} \right) = \lim_{s \rightarrow 0} (t + \mathcal{O}(s)) = t.$$

□

Proof of Proposition 1.

Using $\frac{\partial \hat{f}_\mu(\mathbf{x}^*, \tau)}{\partial \tau} = \frac{\partial \hat{f}(\mathbf{x}^*, \tau)}{\partial \tau} = \mathbf{k}^{*\top} (\mathbf{y} - \hat{\mathbf{f}}(\tau))$ from Equation 3 and $\|\mathbf{y} - \hat{\mathbf{f}}(\tau)\|_2 \leq e^{-\int_0^\tau s_{\min}(\tau_1) d\tau_1} \cdot \|\mathbf{y}_\mu\|_2$ from

Lemma 4, we obtain

$$\begin{aligned}
|\hat{f}_\mu(\mathbf{x}^*, t)| &= \left| \int_0^t \frac{\partial \hat{f}_\mu(\mathbf{x}^*, \tau)}{\partial \tau} d\tau \right| \leq \int_0^t \left| \frac{\partial \hat{f}_\mu(\mathbf{x}^*, \tau)}{\partial \tau} \right| d\tau = \int_0^t \left| \mathbf{k}^*(\tau)^\top (\mathbf{y} - \hat{\mathbf{f}}(\tau)) \right| d\tau \\
&\leq \int_0^t \|\mathbf{k}^*(\tau)\|_2 \cdot \|\mathbf{y} - \hat{\mathbf{f}}(\tau)\|_2 d\tau = \overline{k}_2^*(t) \cdot \int_0^t \|\mathbf{y} - \hat{\mathbf{f}}(\tau)\|_2 d\tau \\
&\leq \overline{k}_2^*(t) \cdot \int_0^t e^{-\int_0^\tau s_{\min}(\tau_1) d\tau_1} d\tau \cdot \|\mathbf{y}_\mu\|_2.
\end{aligned} \tag{18}$$

According to the mean value theorem, on one hand, for some $t' \in [0, t]$,

$$\begin{aligned}
\int_0^t e^{-\int_0^\tau s_{\min}(\tau_1) d\tau_1} d\tau \cdot \|\mathbf{y}_\mu\|_2 &= \int_0^t \frac{1}{-s_{\min}(\tau)} \underbrace{(-s_{\min}(\tau)) \cdot e^{-\int_0^\tau s_{\min}(\tau_1) d\tau_1}}_{\leq 0} d\tau \cdot \|\mathbf{y}_\mu\|_2 \\
&= \frac{1}{-s_{\min}(t')} \cdot \int_0^t (-s_{\min}(\tau)) \cdot e^{-\int_0^\tau s_{\min}(\tau_1) d\tau_1} d\tau \cdot \|\mathbf{y}_\mu\|_2 \\
&= \frac{1}{s_{\min}(t')} \cdot \underbrace{\left(1 - e^{-\int_0^t s_{\min}(\tau) d\tau}\right)}_{\leq 1} \cdot \|\mathbf{y}_\mu\|_2 \leq \frac{1}{s_{\min}(t')} \cdot \|\mathbf{y}_\mu\|_2,
\end{aligned} \tag{19}$$

and on the other hand for some $\tau \in [0, t]$,

$$\int_0^t e^{-\int_0^\tau s_{\min}(\tau_1) d\tau_1} d\tau \cdot \|\mathbf{y}_\mu\|_2 = e^{-\int_0^\tau s_{\min}(\tau) d\tau} \cdot \int_0^t 1 d\tau \cdot \|\mathbf{y}_\mu\|_2 = \underbrace{e^{-\int_0^\tau s_{\min}(\tau) d\tau}}_{\leq 1} \cdot t \cdot \|\mathbf{y}_\mu\|_2 \leq t \cdot \|\mathbf{y}_\mu\|_2. \tag{20}$$

Putting Equations 18, 19, and 20 together, we obtain

$$|\hat{f}_\mu(\mathbf{x}^*, t)| \leq \overline{k}_2^*(t) \cdot \int_0^t e^{-\int_0^\tau s_{\min}(\tau_1) d\tau_1} d\tau \cdot \|\mathbf{y}_\mu\|_2 \leq \overline{k}_2^*(t) \cdot \min\left(t, \frac{1}{s_{\min}(t')}\right) \cdot \|\mathbf{y}_\mu\|_2.$$

□

Lemma 4.

Let $s_{\min}(\tau) = s_{\min}(\mathbf{K}(\tau))$ denote the smallest singular value of $\mathbf{K}(\tau)$ for $\tau \in [0, t]$. Then

$$\left\| \mathbf{y} - \hat{\mathbf{f}}(t) \right\|_2 \leq e^{-\int_0^t s_{\min}(\tau) d\tau} \cdot \|\mathbf{y}_\mu\|_2.$$

Proof.

The proof is an adaptation of the proof of Theorem 8.2 by Rugh (1996).

Let $\hat{\boldsymbol{\eta}}(t) = \mathbf{y} - \hat{\mathbf{f}}(t)$. Then $\hat{\boldsymbol{\eta}}(0) = \mathbf{y}_\mu$ and according to Equation 3,

$$\hat{\boldsymbol{\eta}}'(t) = -\frac{\partial \hat{\mathbf{f}}(t)}{\partial t} = -\mathbf{K}(t) (\mathbf{y} - \hat{\mathbf{f}}(t)) = -\mathbf{K}(t) \hat{\boldsymbol{\eta}}(t).$$

Using the chain rule, we obtain

$$(\|\hat{\boldsymbol{\eta}}(t)\|_2^2)' = (\hat{\boldsymbol{\eta}}(t)^\top \hat{\boldsymbol{\eta}}(t))' = 2\hat{\boldsymbol{\eta}}(t)^\top \hat{\boldsymbol{\eta}}'(t) = -2\hat{\boldsymbol{\eta}}(t)^\top \mathbf{K}(t) \hat{\boldsymbol{\eta}}(t) \leq -2 \cdot s_{\min}(t) \cdot \|\hat{\boldsymbol{\eta}}(t)\|_2^2,$$

where in the last inequality we have used that the Rayleigh quotient of a symmetric matrix, \mathbf{A} , is bounded by its eigenvalues: For all vectors \mathbf{v} ,

$$s_{\min}(\mathbf{A}) \leq \frac{\mathbf{v}^\top \mathbf{A} \mathbf{v}}{\mathbf{v}^\top \mathbf{v}} \leq s_{\max}(\mathbf{A}) \iff s_{\min}(\mathbf{A}) \cdot \|\mathbf{v}\|_2^2 \leq \mathbf{v}^\top \mathbf{A} \mathbf{v} \leq s_{\max}(\mathbf{A}) \cdot \|\mathbf{v}\|_2^2.$$

Using Grönwall's inequality on

$$(\|\hat{\boldsymbol{\eta}}(t)\|_2^2)' \leq -2s_{\min}(t) \cdot \|\hat{\boldsymbol{\eta}}(t)\|_2^2,$$

we obtain

$$\begin{aligned}\|\hat{\boldsymbol{\eta}}(t)\|_2^2 &\leq e^{-2 \int_0^t s_{\min}(\tau) d\tau} \cdot \|\hat{\boldsymbol{\eta}}(0)\|_2^2 \iff \|\hat{\boldsymbol{\eta}}(t)\|_2 \leq e^{-\int_0^t s_{\min}(\tau) d\tau} \cdot \|\hat{\boldsymbol{\eta}}(0)\|_2 \\ &= \underbrace{e^{-\int_0^t s_{\min}(\tau) d\tau}}_{\leq 1} \cdot \|\mathbf{y}_\mu\|_2 \leq \|\mathbf{y}_\mu\|_2.\end{aligned}$$

□

Proof of Proposition 2.

Since $\lim_{\sigma \rightarrow \infty} \mathbf{k}^*(\sigma) = \mathbf{1}$, and $\lim_{\sigma \rightarrow \infty} \mathbf{K}(\sigma) = \mathbf{1}\mathbf{1}^\top$, where $\mathbf{1} \in \mathbb{R}^n$ is a vector of only ones,

$$\begin{aligned}\lim_{\sigma \rightarrow \infty} \hat{f}_\mu(\mathbf{x}^*, t, \sigma) &= \mathbf{1}^\top (\mathbf{1}\mathbf{1}^\top)^{-1} (\mathbf{I} - \exp(-t\mathbf{1}\mathbf{1}^\top)) \mathbf{y}_\mu = \mathbf{1}^\top (\mathbf{1}\mathbf{1}^\top)^{-1} \left(\mathbf{I} - \sum_{k=0}^{\infty} \frac{(-t)^k}{k!} \underbrace{(\mathbf{1}\mathbf{1}^\top)^k}_{=n^{k-1} \cdot \mathbf{1}\mathbf{1}^\top} \right) \mathbf{y}_\mu \\ &= \mathbf{1}^\top (\mathbf{1}\mathbf{1}^\top)^{-1} \left(\mathbf{I} - \frac{1}{n} \cdot \mathbf{1}\mathbf{1}^\top \cdot \sum_{k=0}^{\infty} \frac{(-tn)^k}{k!} \right) \mathbf{y}_\mu = \mathbf{1}^\top \left((\mathbf{1}\mathbf{1}^\top)^{-1} - \frac{1}{n} \cdot e^{-tn} \right) \mathbf{y}_\mu \\ &\stackrel{(a)}{=} \frac{1}{n} \cdot \left(1 - \frac{1}{n} \cdot e^{-tn} \right) \mathbf{1}^\top \mathbf{y}_\mu = (1 - e^{-tn}) \cdot \frac{1}{n} \cdot \sum_{i=1}^n y_{\mu,i} = (1 - e^{-tn}) \cdot \bar{y}_\mu,\end{aligned}$$

where (a) is calculated using the matrix inversion lemma,

$$\mathbf{D}^{-1} \mathbf{C} (\mathbf{A} - \mathbf{B} \mathbf{D}^{-1} \mathbf{C})^{-1} = (\mathbf{D} - \mathbf{C} \mathbf{A}^{-1} \mathbf{B})^{-1} \mathbf{C} \mathbf{A}^{-1},$$

for $\mathbf{A} = \varepsilon \mathbf{I}$, $\mathbf{B} = -\mathbf{1}$, $\mathbf{C} = \mathbf{1}^\top$ and $\mathbf{D} = \mathbf{I}$:

$$\mathbf{1}^\top (\mathbf{1}\mathbf{1}^\top)^{-1} = \lim_{\varepsilon \rightarrow 0} \mathbf{1}^\top (\mathbf{1}\mathbf{1}^\top + \varepsilon \mathbf{I})^{-1} = \lim_{\varepsilon \rightarrow 0} \mathbf{1}^\top (\mathbf{I} + \mathbf{1}^\top (1/\varepsilon) \mathbf{1})^{-1} \mathbf{1}^\top (1/\varepsilon) \mathbf{I} = \lim_{\varepsilon \rightarrow 0} \frac{1}{\varepsilon + n} \mathbf{1}^\top = \frac{1}{n} \cdot \mathbf{1}^\top.$$

Similarly,

$$\begin{aligned}\lim_{\sigma \rightarrow \infty} \hat{f}_\mu(\mathbf{x}^*, \lambda, \sigma) &= \mathbf{1}^\top (\mathbf{1}\mathbf{1}^\top + \lambda \mathbf{I})^{-1} \mathbf{y}_\mu \stackrel{(a)}{=} (\mathbf{I} + \mathbf{1}^\top (1/\lambda) \mathbf{1})^{-1} \mathbf{1}^\top (1/\lambda) \mathbf{y}_\mu \\ &= 1/\lambda (\mathbf{I} + 1/\lambda \mathbf{1}^\top \mathbf{1})^{-1} \mathbf{1}^\top \mathbf{y}_\mu = \frac{1}{\lambda} \cdot \frac{1}{1 + n/\lambda} \cdot \sum_{i=1}^n y_{\mu,i} \\ &= \frac{1}{n + \lambda} \cdot \sum_{i=1}^n y_{\mu,i} = \frac{n}{n + \lambda} \cdot \bar{y}_\mu,\end{aligned}$$

where (a) is according to the matrix inversion lemma for $\mathbf{A} = \lambda \mathbf{I}$, $\mathbf{B} = -\mathbf{1}$, $\mathbf{C} = \mathbf{1}^\top$ and $\mathbf{D} = \mathbf{I}$.

We further have $\lim_{\sigma \rightarrow 0} \mathbf{k}^*(\sigma) = \begin{cases} \mathbf{0} & \text{if } \mathbf{x}^* \notin \mathbf{X} \\ \mathbf{e}_i & \text{if } \mathbf{x}^* = \mathbf{x}_i \in \mathbf{X}, \end{cases}$ where \mathbf{e}_i is a vector of only zeros, except element i which is one, and $\lim_{\sigma \rightarrow 0} \mathbf{K}(\sigma) = \mathbf{I}$.

Thus, if $\mathbf{x}^* \notin \mathbf{X}$,

$$\begin{aligned}\lim_{\sigma \rightarrow 0} \hat{f}_\mu(\mathbf{x}^*, t, \sigma) &= \mathbf{0}^\top (\mathbf{I} - \exp(-t\mathbf{I})) \mathbf{I}^{-1} \mathbf{y}_\mu = 0 \\ \lim_{\sigma \rightarrow 0} \hat{f}_\mu(\mathbf{x}^*, \lambda, \sigma) &= \mathbf{0}^\top (\mathbf{I} + \lambda \mathbf{I})^{-1} \mathbf{y}_\mu = 0.\end{aligned}$$

If $\mathbf{x}^* = \mathbf{x}_i \in \mathbf{X}$,

$$\begin{aligned}\lim_{\sigma \rightarrow 0} \hat{f}_\mu(\mathbf{x}^*, t, \sigma) &= \mathbf{e}_i^\top (\mathbf{I} - \exp(-t\mathbf{I})) \mathbf{I}^{-1} \mathbf{y}_\mu = (1 - e^{-t}) \cdot \mathbf{e}_i^\top \mathbf{y}_\mu = (1 - e^{-t}) \cdot y_{\mu,i} \\ \lim_{\sigma \rightarrow 0} \hat{f}_\mu(\mathbf{x}^*, \lambda, \sigma) &= \mathbf{e}_i^\top (\mathbf{I} + \lambda \mathbf{I})^{-1} \mathbf{y}_\mu = \frac{1}{1 + \lambda} \cdot \mathbf{e}_i^\top \mathbf{y}_\mu = \frac{y_{\mu,i}}{1 + \lambda}.\end{aligned}$$

□

Proof of Proposition 3.

Mimicking the calculations in the proof of Proposition 1, we obtain, for the same $t' \in [0, t]$,

$$\begin{aligned}
\left\| \frac{\partial \hat{f}_\mu(\mathbf{x}^*, t)}{\partial \mathbf{x}^*} \right\|_2 &= \left\| \int_0^t \frac{\partial \hat{f}_\mu(\mathbf{x}^*, \tau)}{\partial \tau \partial \mathbf{x}^*} d\tau \right\|_2 \leq \int_0^t \left\| \frac{\partial \hat{f}_\mu(\mathbf{x}^*, \tau)}{\partial \tau \partial \mathbf{x}^*} \right\|_2 d\tau \\
&= \int_0^t \left\| \frac{\partial}{\partial \mathbf{x}^*} \left(\mathbf{k}(\mathbf{x}^*, \mathbf{X}, \tau)^\top (\mathbf{y} - \hat{\mathbf{f}}(\tau)) \right) \right\|_2 d\tau \leq \int_0^t \left\| \frac{\partial \mathbf{k}(\mathbf{x}^*, \mathbf{X}, \tau)}{\partial \mathbf{x}^*} \right\|_2 \cdot \|\mathbf{y} - \hat{\mathbf{f}}(\tau)\|_2 d\tau \\
&= \frac{\int_0^t \left\| \frac{\partial \mathbf{k}(\mathbf{x}^*, \mathbf{X}, \tau)}{\partial \mathbf{x}^*} \right\|_2 \cdot \|\mathbf{y} - \hat{\mathbf{f}}(\tau)\|_2 d\tau}{\int_0^t \|\mathbf{y} - \hat{\mathbf{f}}(\tau)\|_2 d\tau} \cdot \int_0^t \|\mathbf{y} - \hat{\mathbf{f}}(\tau)\|_2 d\tau \\
&\leq \frac{\int_0^t \left\| \frac{\partial \mathbf{k}(\mathbf{x}^*, \mathbf{X}, \tau)}{\partial \mathbf{x}^*} \right\|_2 \cdot \|\mathbf{y} - \hat{\mathbf{f}}(\tau)\|_2 d\tau}{\int_0^t \|\mathbf{y} - \hat{\mathbf{f}}(\tau)\|_2 d\tau} \cdot \min \left(t, \frac{1}{s_{\min}(t')} \right) \cdot \|\mathbf{y}_\mu\|_2.
\end{aligned}$$

Now, since the covariance matrix $\sigma(\tau)\Sigma$, and thus also $\Theta = \Sigma^{-1}$, is positive definite, $\Theta = \sqrt{\Theta} \cdot \sqrt{\Theta}$ and $\|\sqrt{\Theta}\|_2 = \sqrt{\|\Theta\|_2}$,

$$\begin{aligned}
\left\| \frac{\partial \mathbf{k}(\mathbf{x}^*, \mathbf{X}, \tau)}{\partial \mathbf{x}^*} \right\|_2 &= \left\| \frac{\partial}{\partial \mathbf{x}^*} \left(\left[k \left(\frac{\|\mathbf{x}^* - \mathbf{x}_1\|_\Theta}{\sigma(\tau)} \right), k \left(\frac{\|\mathbf{x}^* - \mathbf{x}_2\|_\Theta}{\sigma(\tau)} \right), \dots, k \left(\frac{\|\mathbf{x}^* - \mathbf{x}_n\|_\Theta}{\sigma(\tau)} \right) \right] \right) \right\|_2 \\
&= \left\| \left[k' \left(\frac{\|\mathbf{x}^* - \mathbf{x}_1\|_\Theta}{\sigma(\tau)} \right) \cdot \frac{1}{\sigma(\tau)} \cdot \frac{\Theta(\mathbf{x}^* - \mathbf{x}_1)}{\|\mathbf{x}^* - \mathbf{x}_1\|_\Theta}, \dots, k' \left(\frac{\|\mathbf{x}^* - \mathbf{x}_n\|_\Theta}{\sigma(\tau)} \right) \cdot \frac{1}{\sigma(\tau)} \cdot \frac{\Theta(\mathbf{x}^* - \mathbf{x}_n)}{\|\mathbf{x}^* - \mathbf{x}_n\|_\Theta} \right] \right\|_2 \\
&= \left\| \frac{\sqrt{\Theta}}{\sigma(\tau)} \cdot \left[k' \left(\frac{\|\mathbf{x}^* - \mathbf{x}_1\|_\Theta}{\sigma(\tau)} \right) \cdot \frac{\sqrt{\Theta}(\mathbf{x}^* - \mathbf{x}_1)}{\|\sqrt{\Theta}(\mathbf{x}^* - \mathbf{x}_1)\|_2}, \dots, k' \left(\frac{\|\mathbf{x}^* - \mathbf{x}_n\|_\Theta}{\sigma(\tau)} \right) \cdot \frac{\sqrt{\Theta}(\mathbf{x}^* - \mathbf{x}_n)}{\|\sqrt{\Theta}(\mathbf{x}^* - \mathbf{x}_n)\|_2} \right] \right\|_2 \\
&\leq \underbrace{\max_u |k'(u)|}_{=: k'_{\max}} \cdot \underbrace{\frac{1}{\sigma(\tau)}}_{\sigma(t) \geq 0} \cdot \|\sqrt{\Theta}\|_2 \cdot \left\| \left[\frac{\sqrt{\Theta}(\mathbf{x}^* - \mathbf{x}_1)}{\|\sqrt{\Theta}(\mathbf{x}^* - \mathbf{x}_1)\|_2}, \dots, \frac{\sqrt{\Theta}(\mathbf{x}^* - \mathbf{x}_n)}{\|\sqrt{\Theta}(\mathbf{x}^* - \mathbf{x}_n)\|_2} \right] \right\|_2 \\
&\leq k'_{\max} \cdot \frac{1}{\sigma(\tau)} \cdot \|\sqrt{\Theta}\|_2 \cdot \left\| \left[\frac{\sqrt{\Theta}(\mathbf{x}^* - \mathbf{x}_1)}{\|\sqrt{\Theta}(\mathbf{x}^* - \mathbf{x}_1)\|_2}, \dots, \frac{\sqrt{\Theta}(\mathbf{x}^* - \mathbf{x}_n)}{\|\sqrt{\Theta}(\mathbf{x}^* - \mathbf{x}_n)\|_2} \right] \right\|_F \\
&= k'_{\max} \cdot \frac{1}{\sigma(\tau)} \cdot \sqrt{n} \cdot \sqrt{\|\Theta\|_2},
\end{aligned}$$

where in the last inequality we used $\|\mathbf{A}\|_2 \leq \|\mathbf{A}\|_F$, and in the last equality we used that each column in the $n \times p$ matrix has Euclidean norm 1.

Thus,

$$\frac{\int_0^t \left\| \frac{\partial \mathbf{k}(\mathbf{x}^*, \mathbf{X}, \tau)}{\partial \mathbf{x}^*} \right\|_2 \cdot \|\mathbf{y} - \hat{\mathbf{f}}(\tau)\|_2 d\tau}{\int_0^t \|\mathbf{y} - \hat{\mathbf{f}}(\tau)\|_2 d\tau} \leq \frac{\int_0^t k'_{\max} \cdot \sqrt{n} \cdot \|\Theta\|_2 \cdot \frac{1}{\sigma(\tau)} \cdot \|\mathbf{y} - \hat{\mathbf{f}}(\tau)\|_2 d\tau}{\int_0^t \|\mathbf{y} - \hat{\mathbf{f}}(\tau)\|_2 d\tau} = k'_{\max} \cdot \sqrt{n} \cdot \|\Theta\|_2 \cdot \overline{\sigma^{-1}}$$

and

$$\left\| \frac{\partial \hat{f}_\mu(\mathbf{x}^*, t)}{\partial \mathbf{x}^*} \right\|_2 \leq \overline{\sigma^{-1}} \cdot \min \left(t, \frac{1}{s_{\min}(t')} \right) \cdot \|\mathbf{y}_\mu\|_2 \cdot k'_{\max} \cdot \sqrt{n} \cdot \|\Theta\|_2.$$

To prove Equation 11, let $\mathbf{x}_\mu^*(t)$ be a value such that $\hat{f}_\mu(\mathbf{x}_\mu^*(t), t) = 0$. Since $\bar{y}_\mu = 0$, due to continuity, such an $\mathbf{x}_\mu^*(t)$ always exists. Then, according to the mean value theorem, for some $\mathbf{x}(t) \in [\mathbf{x}^*, \mathbf{x}_\mu^*(t)]$,

$$\begin{aligned} \left| \hat{f}_\mu(\mathbf{x}^*, t) \right| &= \left| \hat{f}_\mu(\mathbf{x}^*, t) - \hat{f}_\mu(\mathbf{x}_\mu^*(t), t) \right| = \left\| \frac{\partial \hat{f}_\mu(\mathbf{x}(t), t)}{\partial \mathbf{x}(t)} \right\|_2 \cdot \|\mathbf{x}^* - \mathbf{x}_\mu^*(t)\|_2 \\ &\leq \overline{\sigma^{-1}} \cdot \min \left(t, \frac{1}{s_{\min}(t')} \right) \cdot \|\mathbf{y}_\mu\|_2 \cdot k'_{\max} \cdot \sqrt{n \cdot \|\Theta\|_2} \cdot \|\mathbf{x}^* - \mathbf{x}_\mu^*(t)\|_2 \\ &\leq \overline{\sigma^{-1}} \cdot \min \left(t, \frac{1}{s_{\min}(t')} \right) \cdot \|\mathbf{y}_\mu\|_2 \cdot k'_{\max} \cdot \sqrt{n \cdot \|\Theta\|_2} \cdot \|\mathbf{x}^* - \mathbf{x}_m\|_2. \end{aligned}$$

□

Proof of Lemma 2.

Using the chain rule and $\frac{\partial \hat{f}_\mu(t)}{\partial t} = \frac{\partial \hat{\mathbf{f}}(t)}{\partial t} = \mathbf{K}(t) (\mathbf{y} - \hat{\mathbf{f}}(t))$ from Equation 3, we obtain

$$\begin{aligned} \frac{\partial R^2(t)}{\partial t} &= \left(\frac{\partial R^2(t)}{\partial \hat{\mathbf{f}}(t)} \right)^\top \left(\frac{\partial \hat{\mathbf{f}}(t)}{\partial t} \right) = \frac{2 (\mathbf{y} - \hat{\mathbf{f}}(t))^\top}{\|\mathbf{y} - \bar{\mathbf{y}}\|_2^2} \mathbf{K}(t) (\mathbf{y} - \hat{\mathbf{f}}(t)) \\ &= 2 \cdot \frac{\|\mathbf{y} - \hat{\mathbf{f}}(t)\|_{\mathbf{K}(t)}^2}{\|\mathbf{y} - \bar{\mathbf{y}}\|_2^2} \geq 0, \end{aligned}$$

which proves Equation 13.

To prove Equation 14, we first note that

$$\begin{aligned} \frac{\partial R^2(t)}{\partial t} \cdot \frac{1}{2} \cdot \frac{1}{1 - R^2(t)} &= 2 \cdot \frac{\|\mathbf{y} - \hat{\mathbf{f}}(t)\|_{\mathbf{K}(t)}^2}{\|\mathbf{y} - \bar{\mathbf{y}}\|_2^2} \cdot \frac{1}{2} \cdot \frac{\|\mathbf{y} - \bar{\mathbf{y}}\|_2^2}{\|\mathbf{y} - \hat{\mathbf{f}}(t)\|_2^2} \\ &= \frac{(\mathbf{y} - \hat{\mathbf{f}}(t))^\top \mathbf{K}(t) (\mathbf{y} - \hat{\mathbf{f}}(t))}{(\mathbf{y} - \hat{\mathbf{f}}(t))^\top (\mathbf{y} - \hat{\mathbf{f}}(t))}. \end{aligned}$$

Now, the right-hand side of the expression above is the Rayleigh quotient of $\mathbf{K}(t)$, which is bounded by the singular values, i.e. for any vector \mathbf{v} and symmetric matrix \mathbf{A} , $s_{\min}(\mathbf{A}) \leq \frac{\mathbf{v}^\top \mathbf{A} \mathbf{v}}{\mathbf{v}^\top \mathbf{v}} \leq s_{\max}(\mathbf{A})$. Thus,

$$s_{\min}(\mathbf{K}(t)) \leq \frac{\partial R^2(t)}{\partial t} \cdot \frac{1}{2} \cdot \frac{1}{1 - R^2(t)} \leq s_{\max}(\mathbf{K}(t)).$$

Finally, for constant \mathbf{K} ,

$$\begin{aligned} \frac{\partial^2 R^2(t)}{\partial t^2} &= \left(\frac{\partial \frac{\partial R^2(t)}{\partial t}}{\partial \hat{\mathbf{f}}(t)} \right)^\top \left(\frac{\partial \hat{\mathbf{f}}(t)}{\partial t} \right) = \frac{-4 (\mathbf{y} - \hat{\mathbf{f}}(t))^\top \mathbf{K}}{\|\mathbf{y} - \bar{\mathbf{y}}\|_2^2} \cdot \mathbf{K} (\mathbf{y} - \hat{\mathbf{f}}(t)) \\ &= -4 \cdot \frac{\|\mathbf{y} - \hat{\mathbf{f}}(t)\|_{\mathbf{K}^2}^2}{\|\mathbf{y} - \bar{\mathbf{y}}\|_2^2} \leq 0, \end{aligned}$$

which proves Equation 15. □